

# Batch Normalization Decomposed

**Ido Nachum\***

**Marco Bondaschi\***

**Michael Gastpar**

**Anatoly Khina**

inachum@univ.haifa.ac.il

marco.bondaschi@epfl.ch

michael.gastpar@epfl.ch

anatolyk@tauex.tau.ac.il

## Abstract

*Batch normalization* is a successful building block of neural network architectures. Yet, it is not well understood. A neural network layer with batch normalization comprises three components that affect the representation induced by the network: *recentering* the mean of the representation to zero, *rescaling* the variance of the representation to one, and finally applying a *non-linearity*. Our work follows the work of Hadi Daneshmand, Amir Joudaki, Francis Bach [NeurIPS '21], which studied deep *linear* neural networks with only the rescaling stage between layers at initialization. In our work, we present an analysis of the other two key components of networks with batch normalization, namely, the recentering and the non-linearity. When these two components are present, we observe a curious behavior at initialization. Through the layers, the representation of the batch converges to a single cluster except for an odd data point that breaks far away from the cluster in an orthogonal direction. We shed light on this behavior from two perspectives: (1) we analyze the geometrical evolution of a simplified indicative model; (2) we prove a stability result for the aforementioned configuration.

---

\*These authors contributed equally to this work.

## Introduction

A neural network (NN) consists of a sequence of *transformations* or *layers* sharing a similar structure. Typically, the  $t$ -th transformation  $t$ -th transformation comprises two steps:

1. Multiply the output of the previous layer  $\mathbf{x}^{(t-1)}$  by a matrix  $W^{(t)}$ :  $\mathbf{z}^{(t)} = W^{(t)}\mathbf{x}^{(t-1)}$ .
2. Apply a non-linearity  $F : \mathbb{R} \rightarrow \mathbb{R}$  coordinatewise to attain the new output:  $\mathbf{x}^{(t)} = F(\mathbf{z}^{(t)})$ .

In practice, many different tweaks are applied to these transformations to improve performance. Batch normalization (BN) [Ioffe and Szegedy \(2015\)](#) is a prime such example. It is a ubiquitous component of NNs as it decreases the training time and the generalization error [He et al. \(2016\)](#); [Huang et al. \(2017\)](#); [Silver et al. \(2017\)](#). A noteworthy aspect of BN is that the output corresponding to a single input depends on other inputs in the same batch.

Let  $X^{(t)} = \left( \mathbf{x}_1^{(t)} \mid \dots \mid \mathbf{x}_n^{(t)} \right)$  be the output of layer  $t$  consisting of  $n$  column vectors that correspond to a batch of size  $n$ . Then, the output of every layer of a NN with BN is defined recursively as follows.

1. Multiply the output of the previous layer  $X^{(t-1)}$  by a matrix  $W^{(t)}$ :

$$Z^{(t)} = \left( \mathbf{z}_1^{(t)} \mid \dots \mid \mathbf{z}_n^{(t)} \right) := W^{(t)} X^{(t-1)}. \quad (1)$$

2. Compute the empirical mean and standard deviation

$$\boldsymbol{\mu}^{(t)} := \frac{1}{n} \sum_{i=1}^n \mathbf{z}_i^{(t)}, \quad \boldsymbol{\sigma}^{(t)} := \sqrt{\frac{1}{n} \sum_{i=1}^n \left( \mathbf{z}_i^{(t)} - \boldsymbol{\mu}^{(t)} \right)^2}. \quad (2)$$

3. Normalize  $Z^{(t)}$  by *recentering* (RC) and *rescaling* (RS):

$$\bar{Z}^{(t)} = \left( \bar{\mathbf{z}}_1^{(t)} \mid \dots \mid \bar{\mathbf{z}}_n^{(t)} \right) := \frac{Z^{(t)} - \boldsymbol{\mu}^{(t)}}{\boldsymbol{\sigma}^{(t)}} = \left( \frac{\mathbf{z}_1^{(t)} - \boldsymbol{\mu}^{(t)}}{\boldsymbol{\sigma}^{(t)}} \mid \dots \mid \frac{\mathbf{z}_n^{(t)} - \boldsymbol{\mu}^{(t)}}{\boldsymbol{\sigma}^{(t)}} \right). \quad (3)$$

4. Apply a non-linearity (NL)  $F : \mathbb{R} \rightarrow \mathbb{R}$  coordinatewise to the normalized batch  $\bar{Z}^{(t)}$ :

$$X^{(t)} := F\left(\bar{Z}^{(t)}\right). \quad (4)$$

After applying BN during initialization (and training), the distribution of the preactivation values of each neuron has zero mean and unit variance (both during initialization and training). This was the original motivation for BN, namely, to reduce the rate at which the representations through the layers change, or put differently, to reduce the covariate shift [Ioffe and Szegedy \(2015\)](#). Yet, this is not the reason for its success [Santurkar et al. \(2018\)](#), and BN is still not well understood.

In this paper, we follow [Daneshmand et al. \(2020, 2021\)](#) where fully-connected *linear* (no ReLU, sigmoid, etc.) neural networks were studied with only one part of BN applied—RS (part IV of [Figure 1](#)). Under that framework at initialization, it was shown that a full-rank batch becomes orthonormal asymptotically as the depth of the network grows.

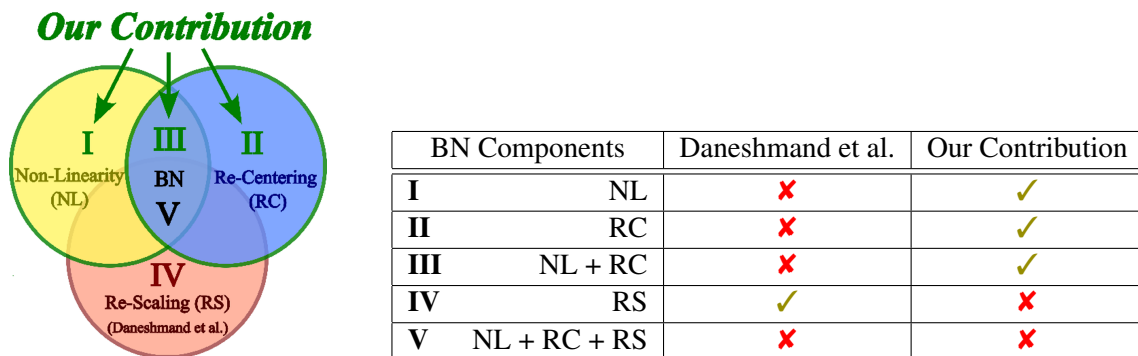


**Figure 1:** A comparison between previous work and our contribution. Our contribution studies the effects of the ReLU non-linearity and recentering at initialization and how they interact.

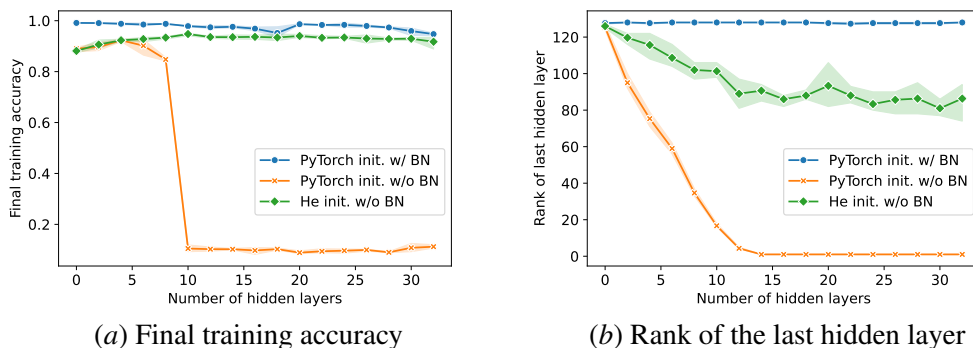
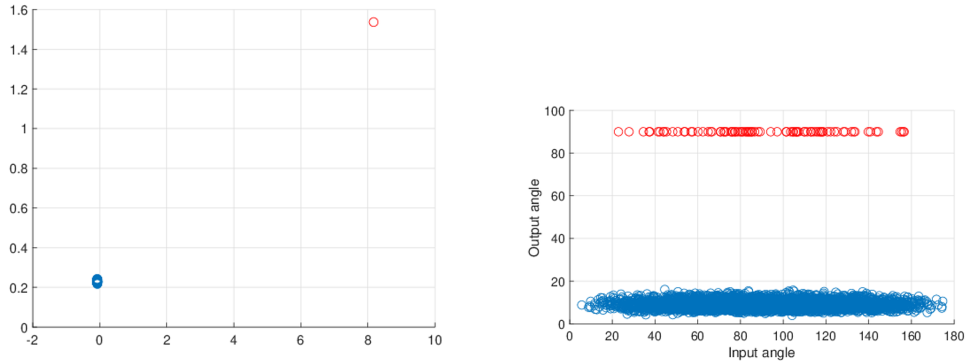


**Figure 2:** Comparison of final training accuracy and the rank of the last hidden layer in a fully-connected ReLU network using the supplementary code of [Daneshmand et al. \(2020\)](#): (1) with BN (2) without BN (3) without BN while changing **only** the default PyTorch initialization in the code to the He initialization.

## Our Contribution

Our contribution begins with a reference to Figure 1 in [Daneshmand et al. \(2020\)](#). That figure suggests that to achieve low training error, NNs must maintain a high rank when representing the training set through the different layers already at initialization (NNs may form low-rank representations at initialization, see [Saxe et al. \(2014\)](#)). Yet, this implication does not hold; see figure 2: a NN may reach high training accuracy from low-rank representations at initialization. To demonstrate this, we set the appropriate He initialization [He et al. \(2015\)](#) (PyTorch’s default variance in the code of [Daneshmand et al. \(2020\)](#) is too small). Figure 2 clearly shows that the success of BN does not stem from a high-rank representation that it induces at initialization and that a more fine-grained approach is required to better understand BN.

Indeed, as we demonstrate in figure 5, with NL the representation achieved by the hidden layers is not orthogonal. The more so, when applying BN without RC, the typical angle between a pair of vectors in say  $\mathbf{x}_1^{(30)}, \dots, \mathbf{x}_n^{(30)}$  (the representation after 30 layers) is approximately  $60^\circ$ —as is evident from Figure 5(a)—as opposed to a typical angle of  $75^\circ$  in the case of BN—as is demonstrated in Figure 5(b). A possible explanation of this difference is offered by Figure 6: when BN without RC is used, the histogram of the activity of some neurons in the network looks like the one shown in Figure 6(a), whereas standard BN with RC induces the same type of histogram as in Figure 6(b) for almost all neurons; untypical histograms, like the one represented in Figure 6(a), induce stronger correlations between inputs and hence the angle between vectors decreases.



(a) 2D projection of the representations. (b) Relation between input and output angles.

**Figure 3:** The batch representation induced by the final hidden layer with RC and ReLU NL. Figure (a) is a random two-dimensional projection of the final layer’s representations. The "escaped" point is marked in red. Figure (b) represents the angles between pairs of vector representations before and after the final layer. The points marked in red represent the angles between the "escaped" point and any other point of the batch.

To understand the effect of each stage of BN, we decompose BN into its three different components (NL, RC, and RS; see Figure 1), and complement the study of Daneshmand et al. (2020, 2021) of RS only, by understanding the role of RC, NL, and how they interact. In correspondence with Figure 1, we focus in Section I on the isolated effect of the ReLU NL on the rank of the representations, where we show that the rank of the representation increases substantially after one layer; in Section II, we focus on the isolated effect of RC and show that in linear networks it affects only the representation of the first layer; in Section III we study the representation induced when combining the randomness of the initialization, NL, and RC; and in the discussion section, we contemplate how all the different pieces of the BN puzzle fit together and suggest an alternative initialization scheme that was inspired by this theoretical work.

Section III is our main contribution, and in its setting, we observe a curious behavior: after enough layers, all the data points in the batch collapse to one point, except for a single odd data point that escapes far away from the cluster in an orthogonal direction. This behavior is illustrated in Figure 3. On a high-level, such behavior may explain the typical histograms that appear for all neurons, as in Figure 6(b), on which we will elaborate further in the Discussion section. We explain the observation above via two theorems:

- Theorem 11 explains the behavior above for a simplified model that is more tractable: At each layer, instead of calculating the expected behavior over the typical Gaussian distribution over the weights, we analyze the expected behavior over a simpler distribution. We show that this simplified model captures the empirical behavior well.
- Theorem 14 deals with Gaussian random layers and provides a stability result. It states that an initial configuration that consists of a cluster and one separate data point, as above, remains geometrically unchanged after the application of a randomly initialized network with RC and ReLU activation.

**All the proofs of the theorems can be found in the Appendix.**

### Notation

Matrices are denoted by capital letters such as  $X$ . For a matrix  $X$ , its  $i$ -th row is denoted by  $\mathbf{x}_i$ , and its  $i$ -th column by  $\mathbf{x}_i$ . Element  $(i, j)$  of  $X$  is denoted by  $X_{ij}$ . The  $i$ -th element of a vector  $\mathbf{y}$  is denoted by  $y_i$ .

The result of the operation denoted by  $X - \boldsymbol{\mu}$ , where  $X$  is a  $d \times n$  matrix, and  $\boldsymbol{\mu}$  is a  $d \times 1$  column vector, is understood to be equal to a  $d \times n$  matrix  $Z$  whose elements are  $Z_{ij} = X_{ij} - \mu_i$ . Similarly, the result of the operation  $\frac{X}{\boldsymbol{\sigma}}$ , where  $X$  is a  $d \times n$  matrix, and  $\boldsymbol{\sigma}$  is a  $d \times 1$  column vector, is understood to be equal to a  $d \times n$  matrix  $Z$  whose elements are  $Z_{ij} = \frac{X_{ij}}{\sigma_i}$ . The result of the operation  $F(X)$ , where  $X$  is a matrix and  $F : \mathbb{R} \rightarrow \mathbb{R}$  is a function, is a matrix  $Z$  with elements  $Z_{ij} = F(X_{ij})$ .

### Related Work

We mention some related works that attempt to understand the underlying principle of BN both theoretically and empirically.

[Karakida et al. \(2019\)](#); [Arora et al. \(2019\)](#); [Bjorck et al. \(2018\)](#); [Lyu et al. \(2022\)](#) studied some beneficial properties of BN to explain its success, [Frankle et al. \(2020\)](#) trained NNs where only the tunable parameters of BN are trained, achieving surprisingly good results, and [Lubana et al. \(2021\)](#) tried to underpin some of the qualities of normalization layers in general.

[Yang et al. \(2019\)](#) studied Deep NNs with BN and without residual connections and explained why they are hard to train; [Furusho and Ikeda \(2020\)](#) and [De and Smith \(2020\)](#) further elaborated on the synergy between skip connections and BN.

Empirically, [Wang et al. \(2022\)](#) highlighted some of the shortcomings of BN in the Transformers architecture, and [Li et al. \(2019\)](#) pointed out some of the shortcomings of BN when used with dropout.

## I. ReLU NL Increases Rank

[Daneshmand et al. \(2020, 2021\)](#) study *linear* networks (i.e., without NL) for which, to reach orthonormality of the vectors within the batch, the input batch needs to be assumed to be full rank. This is because the rank of the batch representations cannot increase through the layers, since  $\text{rank}(AB) \leq \max(\text{rank}(A), \text{rank}(B))$ . In contrast, in a real setting, the NL increases the rank of the batch through the layers. We prove this phenomenon in Theorem 3, which states that applying a random matrix followed by a ReLU NL over the training set induces full rank under a mild assumption. Hence, the NL provides a natural way to increase the dimension of the representations  $X^{(t)}$  of the batch at initialization. Theorem 3 uses the following geometrical quantity.

**Definition 1** Let  $X = (\mathbf{x}_1 | \dots | \mathbf{x}_n) \in \mathbb{R}^{k \times n}$  be a  $k$ -dimensional batch of size  $n$ . We say that the row vectors  $\mathbf{w}_1, \mathbf{w}_2 \in \mathbb{R}^k$  are equivalent,  $\mathbf{w}_1 \sim \mathbf{w}_2$ , if  $\text{sign}(\mathbf{w}_1 \mathbf{x}_i) = \text{sign}(\mathbf{w}_2 \mathbf{x}_i)$  for all  $1 \leq i \leq n$ . We denote the finite set of equivalence classes induced by this relation by  $\{\Gamma_l\}$  and define

$$\gamma(X) = \min\{\text{vol}(\Gamma_l) : \text{vol}(\Gamma_l) > 0\} \quad (5)$$

where  $\text{vol}(\Gamma_l) = \mathbb{P}(\mathbf{w} \in \Gamma_l)$  for  $\mathbf{w} \sim \mathcal{N}(0, I_k)$ .

**Example** Let  $X = (\mathbf{x}_1 | \dots | \mathbf{x}_n)$  such that  $\mathbf{x}_i = (\cos(2\pi i/n), \sin(2\pi i/n))^T$  for  $i \in [n]$  with odd  $n$ . That is,  $X$  is composed of  $n$  equally spaced points on the unit circle. It is clear that  $|\{\text{vol}(\Gamma_l) : \text{vol}(\Gamma_l) > 0\}| = n$  and  $\gamma(X) = 1/n$ .

To prove theorem 3 below, we will use the following lemma.

**Lemma 2** Let  $\mathbf{x}_1, \mathbf{x}_2, \dots, \mathbf{x}_{t+1} \in \mathbb{R}^k$  be column vectors such that no two vectors are collinear. Denote  $X^{(\ell)} := (\mathbf{x}_1 | \mathbf{x}_2 | \dots | \mathbf{x}_\ell)$  for  $\ell \in [t+1]$ . Denote further  $W^{(r)} \in \mathbb{R}^{r \times k}$ , and assume that  $\text{rank}(\text{ReLU}(W^{(r)} X^{(t)})) = t$ . Then, with probability at least  $\gamma(X^{(t+1)})$ ,

$$\text{rank}\left(\text{ReLU}\left(W^{(r+1)} X^{(t+1)}\right)\right) = t + 1, \quad (6)$$

where  $W^{(r+1)} = \begin{bmatrix} W^{(r)} \\ \mathbf{w}_{r+1} \end{bmatrix}$  for  $\mathbf{w}_{r+1} \sim \mathcal{N}(0, I_k)$ .

**Theorem 3** Let  $X \in \mathbb{R}^{k \times n}$  be a  $k$ -dimensional batch of size  $n$  and assume that no two columns of  $X$  are collinear. Let  $W \in \mathbb{R}^{\infty \times k}$  be a random matrix with a countably infinite number of rows, each of size  $k$  and i.i.d. entries  $\mathcal{N}(0, 1)$ . Define  $W^{(d)}$  as the first  $d$  rows of  $W$ ,  $y := \min\{d : \text{rank}(\text{ReLU}(W^{(d)} X)) = n\}$ , and  $\gamma := \gamma(X)$ . Then,

1.  $\mathbb{E}[y] \leq n/\gamma$ .
2. For  $d = \alpha n/\gamma$  for some  $\alpha > 2$ ,

$$\mathbb{P}\left(\text{rank}(\text{ReLU}(W^{(d)} X)) = n\right) \geq 1 - \exp\left\{-n\left(\frac{\alpha}{\gamma} \log \frac{1}{\alpha} + \left(\frac{\alpha}{\gamma} - 1\right) \log \frac{\alpha - \gamma}{1 - \gamma}\right)\right\} \quad (7a)$$

$$\geq 1 - \exp\{-n(\alpha - 1 - \log \alpha)\}. \quad (7b)$$

The theorem states that at most  $n/\gamma(X)$  ReLU neurons are required, in expectation, to guarantee that a representation of any batch will be full rank (item 1), and the probability of not achieving this decays exponentially fast in  $\alpha$  for  $\frac{\alpha n}{\gamma}$  neurons (item 2). The theorem still holds when BN is applied before ReLU, as stated in the next corollary. The proof of the corollary is left to the reader.

**Corollary 4** Theorem 3 holds for  $y := \min\{d : \text{rank}(\text{ReLU}(BN(W^{(d)} X))) = n\}$ , where  $BN$  refers to recentering and rescaling and  $\gamma := \gamma(X - \frac{1}{n} \sum_{i=1}^n \mathbf{x}_i)$ .

Let us now compare Theorem 3 to Lemma 5 in Dittmer et al. (2020). The authors generalize the notion of singular values of linear operators to ReLU neural layers and show that the singular values do not increase for such ReLU operators. Theorem 3 shows that such a generalization does not capture the spirit of singular values for the following reason. The number of non-zero singular values of an operator equals the dimension of its image. So, for example, by Lemma 5 in Dittmer et al. (2020), for a linear operator followed by ReLU with input dimension 2, the maximal number of non-zero singular values is 2. This would suggest that the image dimension of the operator is at most 2. Theorem 3 shows that, in fact, the image dimension scales linearly with the number of rows, so there should be many more non-zero singular values for a generalization of singular values of a ReLU layer.

## II. Recentring

For completeness, we refer briefly to the simple scenario where we use only RC over a linear network. When using RC alone without NL, the representation changes only at the first layer, where the mean is set to zero in every coordinate, and this is maintained through the layers because the mean of every coordinate remains zero after applying the following linear layers. That is, if  $\sum_i \mathbf{x}_i = \mathbf{0}$ , then  $\sum_i W \mathbf{x}_i = \mathbf{0}$  for any  $W$ . Therefore, when used alone, RC does not have any effect on the batch representation after the first layer.

## III. Recentring Followed by ReLU NL

In contrast to the previous section, RC has an effect through all the layers when it is followed by a ReLU NL. Figure 3 displays a behavior that is consistent for all the batches that we experimented with: after enough layers, all of the data points collapse to a single cluster, and one *odd* data point deviates far away, in an orthogonal direction to the cluster.

Let us give a high-level intuition about why the representation in Figure 3 emerges. Assume there is one data point, say  $\mathbf{x}_1$ , that is far, to some degree, from the mean of the rest of the datapoints, namely, from the center of the cluster  $\boldsymbol{\nu} := \frac{1}{n-1} \sum_{i=2}^n \mathbf{x}_i$ . Over each layer, we expect the following to occur:

1. We project the datapoints by a random  $\mathbf{w}$  and expect the distance between the projected  $\mathbf{x}_1$  and the projected  $\boldsymbol{\nu}$  to remain large.
2. We then subtract the projected mean of all datapoints  $\mu := \frac{1}{n} \sum_{i=1}^n \mathbf{w} \mathbf{x}_i$ .  
If  $\mathbf{w} \boldsymbol{\nu} - \mu < 0$ , then  $\mathbf{w} \mathbf{x}_1 - \mu > 0$  and it is likely that many points in the cluster now have negative entries.  
If  $\mathbf{w} \boldsymbol{\nu} - \mu > 0$ , then  $\mathbf{w} \mathbf{x}_1 - \mu < 0$  and it is likely that only few points in the cluster now have negative entries.
3. We apply ReLU to the datapoints.  
If  $\mathbf{w} \boldsymbol{\nu} - \mu < 0$ , then the points in the cluster with negative entries all map to zero. We get a tighter cluster, while the value of the projected odd point does not change.  
If  $\mathbf{w} \boldsymbol{\nu} - \mu > 0$ , then  $\mathbf{x}_1$  maps to zero with a few points from the cluster and the values of other points do not change.

In total, the effect on the representation of a projection with  $\mathbf{w} \boldsymbol{\nu} - \mu > 0$  is much greater than the case with  $\mathbf{w} \boldsymbol{\nu} - \mu < 0$  since in the former case much more points map to zero compared to a selected few in the latter (so the geometry does not change much on average). Hence, when moving from layer to layer, we expect the cluster to become tighter and move closer to zero fast, and the ratio between the representation of  $\mathbf{x}_1$  and the mean of the cluster to become large. This effectively reproduces the geometry in Figure 3.

A typical approach for explaining such behavior would follow two steps. First, for a single ReLU neuron with a corresponding row of weights  $\mathbf{w}$ , calculate what would happen in expectation for the representation of the batch. Secondly, show that this behavior is concentrated around that mean when using many neurons.

For calculating the expectation, we are required to compute

$$\mathbb{E}_{\mathbf{w} \sim \mathcal{N}(0, I_d)} \operatorname{ReLU} \left( \mathbf{w} \left( \mathbf{x}_i - \frac{1}{n} \sum_{r=1}^n \mathbf{x}_r \right) \right) \operatorname{ReLU} \left( \mathbf{w} \left( \mathbf{x}_j - \frac{1}{n} \sum_{r=1}^n \mathbf{x}_r \right) \right). \quad (8)$$

This is the expected inner product between inputs  $\mathbf{x}_i$  and  $\mathbf{x}_j$  after a single layer, which appears to be intractable while keeping tabs over the mean  $\frac{1}{n} \sum_{r=1}^n \mathbf{x}_r^{(t)}$  from layer to layer. This is why we separate our analysis into two theorems. Theorem 11 shows how the representation in Figure 3 emerges under a simplified model, and Theorem 14 shows that such a representation remains invariant under the typical setting, as in equation 8.

### Simplified Model for Recentering + ReLU

We suggest a simplified model to explain the behavior of Figure 3. We start by noting that ReLU is homogeneous. That is,  $\operatorname{ReLU}(\alpha x) = \alpha \operatorname{ReLU}(x)$  for  $\alpha \geq 0$ . Hence, instead of calculating the mean over all projections  $\mathbf{w}$  in  $\mathbb{R}^d$ , as in equation (8), we can calculate the mean over the unit sphere  $\mathbb{S}^{d-1}$ . Another simplification that we use is averaging over all standard unit vectors and their inverses  $S_d := \{e_1, \dots, e_d, -e_1, \dots, -e_d\}$  instead of averaging over all possible angles:

$$\mathbb{E}_{\mathbf{w} \sim \mathcal{N}(0, I_d)} [\cdot] \implies \mathbb{E}_{\mathbf{w} \sim U(\mathbb{S}^{d-1})} [\cdot] \implies \mathbb{E}_{\mathbf{w} \sim U(S_d)} [\cdot]$$

At first glance, the computation  $\mathbb{E}_{\mathbf{w} \sim U(S_d)} [\cdot]$  may seem too simplistic. For example, if we start with a three-dimensional data set, we need to sum only 6 terms. Yet, when we follow this model through many layers, we get an exponential build-up in complexity. In fact, the output of every new layer of the network consists of all possible projections in  $S_d$  of the output of the previous layer. Therefore, the number of summands doubles with each layer: if the batch representation has dimension  $d$ , then after one layer, its dimension increases to  $2d$  (since  $|S_d| = 2d$ ) after two layers—to  $2^2d$ , and after  $t$  layers—to  $2^t d$ . In each step of the process, which corresponds to a layer, we project each dimension  $i$  of the input representation onto the unit vectors  $e_i$  and  $-e_i$ . This is why we can visualize this branching process as a (perfect) binary tree, where each vertex of depth  $t$  represents a neuron of the  $t$ -th layer of the network, see Figure 4 below.

This model has a nice property: in contrast to the general model, which is induced by equation (8), in the simplified case, we can easily keep track of the effect of each neuron in the network (or vertex in the tree) on the representation induced by each layer. This holds because the output of each neuron depends only on its parent neuron from the previous layer. This means that for any branch that begins on some vertex in the tree, its analysis is independent of all the other disjoint branches; this makes the analysis tractable.

That said, if we start with input dimension  $d > 1$ , we will have  $d$  disjoint trees with no interaction between them. So separating the dimensions would yield a different odd point on every coordinate, and no unique odd point can be identified from the batch. It is worth mentioning that no odd point can be identified for Gaussian matrices if our batch is symmetric; in this case, we must wait until the randomness, from layer to layer, will artificially produce an outlier.

Consequently, we work in our model with input dimension  $d = 1$ . That is,  $X^{(0)}$  is a row vector with  $n$  elements. In this case, we can identify the odd point. If  $X^{(0)}$  is ordered, it would be either  $x_1$  or  $x_n$ , and we can rigorously prove the high-level intuition, as in items 1, 2, and 3 above.



**Remark** Empirically, we observe that the odd point would typically be the one with the largest norm. This is compatible with the description above. So analogously, our Theorem 11 holds for input dimension  $d > 1$  under the condition that there are two points such that for each coordinate: (1) the entries of one point are greater than all other entries; (2) the entries of the second point are smaller than all other entries.

Let us now introduce our model and let  $X^{(t)}$  be the representation of the batch at layer  $t$ . Since the starting batch is made up of  $n$  one-dimensional points,  $X^{(0)}$  is a row vector with  $n$  elements, and, due to the branching process described above, in general,  $X^{(t)}$  is a matrix of size  $2^t \times n$ . Each of its columns, which we denote by  $\mathbf{x}_i^{(t)}$  for  $i \in \{1, 2, \dots, n\}$ , is the representation of one data point at layer  $t$  of the network. Each of its rows, which we denote by  $\mathbf{x}_j^{(t)}$  for  $j \in \{1, 2, \dots, 2^t\}$ , represents the output of one neuron at layer  $t$  of the network. The projection of  $X^{(t)}$  over all standard unit vectors and their inverses, i.e., over all vectors in  $S_{2^{t+1}}$ , is exactly equivalent to performing the matrix multiplication  $W^{(t+1)}X^{(t)}$ , where

$$W^{(t+1)} = \begin{pmatrix} +I_{2^t} \\ -I_{2^t} \end{pmatrix}, \quad (9)$$

and  $I_d$  is the identity matrix of size  $d$ . In fact, for every  $i \in \{1, 2, \dots, 2^t\}$ , the output of neuron  $i$ , that is, the  $i$ -th row of  $X^{(t)}$ , generates two neurons' outputs at the next layer, one corresponding to the projection according to  $e_i$ , and the other according to  $-e_i$ . After the projections, RC, and the ReLU non-linearity are applied to each neuron's output. The result is the batch representation at layer  $t + 1$ ,  $X^{(t+1)}$ , which is therefore given by the equation

$$X^{(t+1)} = \text{ReLU} \left( W^{(t+1)} \left( X^{(t)} - \bar{\mathbf{x}}^{(t)} \right) \right), \quad (10)$$

where  $\bar{\mathbf{x}}^{(t)} = \frac{1}{n} \sum_{i=1}^n \mathbf{x}_i^{(t)}$ .

It is clear from the given description that the evolution of each neuron's output from layer  $t$  to  $t + 1$  does not depend in any way on the other neurons of that layer. Hence, we can focus on each neuron independently. In particular, we can say that, for every  $i$ , the output of neuron  $i$ , i.e.,  $\mathbf{x}_i^{(t)}$ , undergoes two different transformations, a *positive* one, which consists of the projection according to  $e_i$  followed by RC and ReLU, and a *negative* one, which comprises the projection according to  $-e_i$ , RC and ReLU. The following is a formal definition of these two transformations.

**Definition 5 (positive and negative transformations)** We say that  $\mathbf{y} \in \mathbb{R}^n$  is the result of a positive transformation applied on  $\mathbf{x} \in \mathbb{R}^n$  if  $y_i = \text{ReLU}(x_i - \bar{x})$  for every  $i \in [n]$ , where  $\bar{x} = \frac{1}{n} \sum_{i=1}^n x_i$ . We say that  $\mathbf{y} \in \mathbb{R}^n$  is the result of a negative transformation applied on  $\mathbf{x} \in \mathbb{R}^n$  if  $y_i = \text{ReLU}(-x_i + \bar{x})$  for every  $i \in [n]$ .

A visual representation of the described process as a binary tree is shown in Figure 4, where each node of the tree represents the output of the corresponding neuron, and each edge connects each output with the two outputs generated at the next layer after the positive and negative transformations.

The first result that we will present about our model is that the outputs of the neurons get more and more clustered as we go through the layers of the network. Therefore, the following definition will be useful.

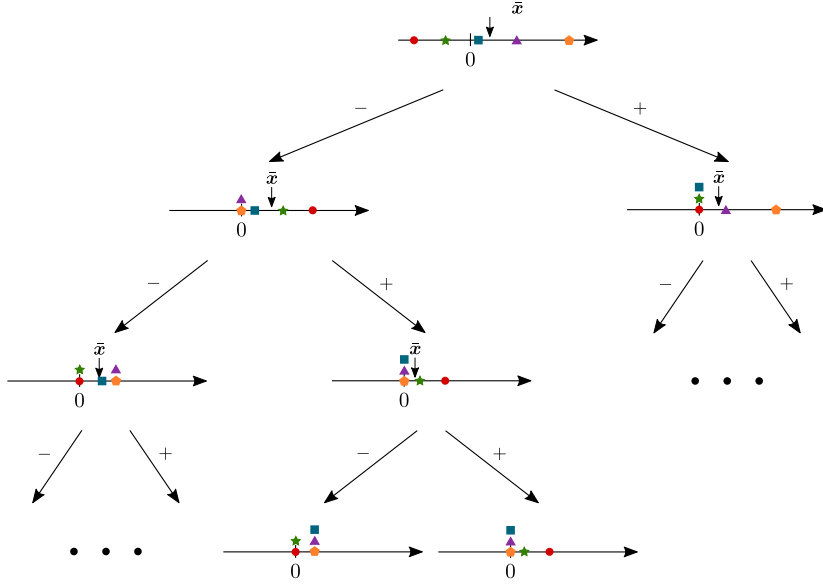


**Figure 4:** Partial example of the first three layers of the tree generated by the process of positive/negative transformations analyzed in this paper, starting from a one-dimensional batch with  $n = 5$  elements. Different elements have different shapes, to make it easier to follow their change of position. The average of the vector at each step is denoted by  $\bar{x}$ .

**Definition 6** A vector  $\mathbf{x} = (x_1, x_2, \dots, x_n) \in \mathbb{R}^n$  with possibly repeated entries is composed of  $k$  clusters if it contains exactly  $k$  unique entries. Denote the sequence of those unique  $k$  entries of  $\mathbf{x}$  in ascending order by  $C(\mathbf{x}) := (c_1(\mathbf{x}), c_2(\mathbf{x}), \dots, c_k(\mathbf{x}))$ , and its length—by  $c(\mathbf{x}) := |C(\mathbf{x})|$ ; clearly,  $k \leq n$ .

The following result is immediate.

**Lemma 7** Let  $y_i = f(x_i)$  for all  $i \in [n]$  for some deterministic function  $f$ . Then,  $c(\mathbf{y}) \leq c(\mathbf{x})$ .

Further, we will show that, as we proceed along the network layers, the number of clusters in each neuron's output will converge to either 2 or 3. Hence, the following definitions are natural.

**Definition 8 (stable)** A vector  $\mathbf{x} \in \mathbb{R}^n$  is stable if  $c(\mathbf{x}) \leq 3$ .

**Definition 9 (more clustered)** A vector  $\mathbf{x} \in \mathbb{R}^n$  is more clustered than a vector  $\mathbf{y} \in \mathbb{R}^n$  if  $c(\mathbf{x}) < c(\mathbf{y})$ .

With these definitions available, we are ready to present the first result of this section, on the clustering of the neurons' outputs.

**Theorem 10** Suppose that a vector  $\mathbf{x}^{(0)} \in \mathbb{R}^n$  with all distinct components undergoes an infinite sequence of positive or negative transformations, resulting in the sequence of vectors  $\{\mathbf{x}^{(t)}\}_{t \geq 0}$ , viz., for every  $t \geq 0$ ,  $\mathbf{x}^{(t+1)}$  is the result of a positive or a negative transformation applied on  $\mathbf{x}^{(t)}$ . Then, there exists a finite  $t_0 \geq 0$  such that  $\mathbf{x}^{(t_0)}$  is stable.

Essentially, Theorem 10 says that, under our simplified model, there is a layer  $t_0$  in the network after which each neuron's output, i.e., each row  $\mathbf{x}_i^{(t)}$  of the matrix  $X^{(t)}$ , for every  $t \geq t_0$ , is a vector composed of at most 3 clusters. This is because, at any layer, each neuron's output is generated by a sequence of positive and negative transformations starting from  $X^{(0)}$ .

Our next step is to study the asymptotic geometry of the batch as the number of layers increases. In particular, we want to study the behavior of the (normalized) inner product between any two datapoint representations, i.e., any two columns  $\mathbf{x}_i^{(t)}$  of  $X^{(t)}$ , when the number of layers goes to infinity. Formally, for any  $i, j \in \{1, 2, \dots, n\}$ , we are interested in the quantity

$$\angle(\mathbf{x}_i^{(t)}, \mathbf{x}_j^{(t)}) := \arccos \frac{\langle \mathbf{x}_i^{(t)}, \mathbf{x}_j^{(t)} \rangle}{\|\mathbf{x}_i^{(t)}\| \cdot \|\mathbf{x}_j^{(t)}\|} \quad (11)$$

in the limit of  $t \rightarrow \infty$ , where  $\mathbf{x}_i^{(t)}$  is the  $i$ -th column of  $X^{(t)}$ , and  $\langle \cdot, \cdot \rangle$  and  $\|\cdot\|$  denote the standard Euclidean inner product and norm, respectively. To that end, we prove the following theorem.

**Theorem 11** *Let  $X^{(0)} \in \mathbb{R}^n$  be a row vector with all distinct components, and assume, without loss of generality, that its entries are increasingly ordered. Let  $X^{(t)}$  be the  $2^t \times n$  matrix defined in equation (10) for  $t \in \mathbb{N}$ , and denote its  $i$ -th column by  $\mathbf{x}_i^{(t)}$ . Then, the following facts are always true.*

1.  $\angle(\mathbf{x}_1^{(t)}, \mathbf{x}_n^{(t)}) = \pi/2$  for all  $t \in \mathbb{N}$ .
2.  $\lim_{t \rightarrow \infty} \angle(\mathbf{x}_i^{(t)}, \mathbf{x}_j^{(t)}) = 0$  for all  $i, j \in \{2, \dots, n-1\}$ .
3. For any  $i \in \{2, \dots, n-1\}$ , either  $\lim_{t \rightarrow \infty} \frac{\|\mathbf{x}_i^{(t)}\|}{\|\mathbf{x}_1^{(t)}\|} \leq \frac{3}{n-2}$  or  $\lim_{t \rightarrow \infty} \frac{\|\mathbf{x}_i^{(t)}\|}{\|\mathbf{x}_n^{(t)}\|} \leq \frac{3}{n-2}$ .
4. For any  $i \in \{2, \dots, n-1\}$ , either

$$\frac{\pi}{2} - \frac{\sqrt{2}\pi}{n-2} \leq \lim_{t \rightarrow \infty} \angle(\mathbf{x}_i^{(t)}, \mathbf{x}_1^{(t)}) \leq \frac{\pi}{2} \quad \text{or} \quad \frac{\pi}{2} - \frac{\sqrt{2}\pi}{n-2} \leq \lim_{t \rightarrow \infty} \angle(\mathbf{x}_i^{(t)}, \mathbf{x}_n^{(t)}) \leq \frac{\pi}{2}. \quad (12)$$

*Interpretation of the theorem.* The theorem shows that, if a one-dimensional batch  $X^{(0)}$  evolves according to our model, after a number of layers large enough, the vector representations of the data points converge to a configuration with the following properties: the representations of the largest and smallest starting datapoints become orthogonal (item 1 of the Theorem); the datapoint representations are all clustered together except for one or two points (item 2); one of the points "escapes" far away from the other clustered points, in such a way that the ratio between the norm of the escaped point and that of any point in the cluster is  $\Theta(n)$  (item 3), and the angle between the escaped point and the cluster is approximately  $90^\circ$  (item 4).

It is important to note that this behavior, derived from the simplified model described at the beginning of the section, is remarkably similar to what happens in the general case of a network with random weights, recentering, and ReLU non-linearity. This behavior, which we described in the introduction, is depicted in Figure 3 above. Hence, our model, even if simpler (and easier to analyze), approximates well the geometrical evolution of a batch in the general random case.

## An Invariant Geometry for Recentering Followed by ReLU

The following definition is an obvious candidate for an invariant representation under RC+ReLU. It consists of one odd point and a cluster where all points are identical. The cluster and the odd point are orthogonal, and the cluster has a much smaller norm. Such a configuration closely resembles the kind of geometrical structure that we see in practice, see Figure 3.

**Definition 12 (invariant representation)** Let  $X^{(t)} = (\mathbf{x}_1 | \dots | \mathbf{x}_n) \in \mathbb{R}^{k \times n}$  be a representation of a  $d$ -dimensional batch of size  $n$  at layer  $t$ , and denote  $\boldsymbol{\nu}_c := \frac{1}{n-1} \sum_{i=2}^n \mathbf{x}_i$ . We say that  $X^{(t)}$  is an invariant representation under RC+ReLU if all the following relations hold.

1.  $\|\mathbf{x}_1\|^2 = 1$ .
2.  $\|\boldsymbol{\nu}_c\|^2 = \frac{1}{(n-1)^2}$ .
3.  $\mathbf{x}_1 \cdot \boldsymbol{\nu}_c = 0$ .
4.  $\mathbf{x}_i = \boldsymbol{\nu}_c$  for all  $2 \leq i \leq n$ .

The following theorem shows that definition 12 indeed makes sense: it states that, in expectation, the invariant representation is indeed invariant under an appropriate initialization variance.

**Theorem 13** Let  $X^{(t)} = (\mathbf{x}_1 | \dots | \mathbf{x}_n) \in \mathbb{R}^{k \times n}$  be an invariant representation under RC+ReLU, and let  $X^{(t+1)} = \text{ReLU}(WX^{(t)} - \boldsymbol{\mu}^{(t)})$  and  $\hat{\boldsymbol{\nu}}_c := \text{ReLU}(W\boldsymbol{\nu}_c - \boldsymbol{\mu}^{(t)})$ , where  $\boldsymbol{\mu}^{(t)} = \frac{1}{n} \sum_{i=1}^n W\mathbf{x}_i^{(t)}$ . Then,  $\mathbb{E}[X^{(t+1)}]$  is also an invariant representation under RC+ReLU, where the expectation is over the  $d \times k$  matrix  $W$  with i.i.d.  $\mathcal{N}(0, \sigma^2)$  entries with  $\sigma^2 = \frac{2\alpha}{d}$  and  $\alpha = \frac{n^2}{n^2 - 2n + 2}$ .

Finally, the following theorem shows that when starting from a representation somewhat similar to an invariant representation, the next layer brings us closer to an invariant representation in expectation. This is true since items 1–4 in Definition 12 correspond to items 1–4 in Theorem 14. As the correspondence between items 1–3 is natural, we focus on item 4. Indeed, after passing through a layer, it is not likely that the cluster would collapse to a single point as in Definition 12. Nonetheless, item 4 shows that the cluster contracts, while keeping the scale of the representation of  $\mathbf{x}_1$  the same.

**Theorem 14** Let  $X^{(t)} = (\mathbf{x}_1 | \dots | \mathbf{x}_n) \in \mathbb{R}^{k \times n}$  be an invariant representation such that  $\|\mathbf{x}_1 - \boldsymbol{\nu}_c\| = R > \frac{n}{n-1}$ , and  $\|\mathbf{x}_i - \boldsymbol{\nu}_c\| < 1/n^2$  for all  $2 \leq i \leq n$ . Then, for

$$X^{(t+1)} = \left( \mathbf{x}_1^{(t+1)} \mid \dots \mid \mathbf{x}_n^{(t+1)} \right) := \text{ReLU} \left( WX^{(t)} - \boldsymbol{\mu}^{(t)} \right) \quad \text{and} \quad \hat{\boldsymbol{\nu}}_c := \text{ReLU} \left( W\boldsymbol{\nu}_c - \boldsymbol{\mu}^{(t)} \right),$$

the following relations hold.

1.  $\mathbb{E} \left[ \left\| \mathbf{x}_1^{(t+1)} \right\| \right] = 1$ .
2.  $\mathbb{E} \left[ \left\| \hat{\boldsymbol{\nu}}_c \right\| \right] = \frac{1}{n-1}$ .
3.  $\mathbf{x}_1^{(t+1)} \cdot \hat{\boldsymbol{\nu}}_c = 0$  (This holds for any  $W$  and not only in expectation).
4. Denote  $\mathbf{x}_{n+1} := \boldsymbol{\nu}_c$  and  $\mathbf{x}_{n+1}^{(t+1)} := \hat{\boldsymbol{\nu}}_c$ . Then,  $\mathbb{E} \left[ \left\| \mathbf{x}_i^{(t+1)} - \mathbf{x}_j^{(t+1)} \right\|^2 \right] < \|\mathbf{x}_i - \mathbf{x}_j\|^2$  for all  $2 \leq i, j \leq n+1$  such that  $\mathbf{x}_i^{(t+1)} \neq \mathbf{x}_j^{(t+1)}$ .

where the expectations are with respect to the  $d \times k$  matrix  $W$  whose entries are i.i.d.  $\mathcal{N}(0, \sigma^2)$  with  $\sigma^2 = \frac{2\alpha}{d}$  and  $\alpha = \frac{n^2}{(n-1)^2 R^2}$ .

## Discussion

It remains to be seen how all the different components of BN interact with one another and what are the exact properties that are responsible for the success of BN. Observing the histogram in Figure 6(b) and combining it with the insights appearing in this paper and previous work, we explore a new initialization scheme: The histogram in Figure 6(b) implies that the neuron is mostly inactive or with small intensity for most inputs.

Our work shows that with no rescaling and at initialization, neurons are active with a large intensity only for the odd data point. Combining this understanding with the insight that orthogonal representations might be beneficial, suggests associating every data point with a unique neuron. That neuron will fire only for its associated input. This way, we attain an orthogonal representation and sparse activity in the network, as we observe in our work.

Initial experimentation suggests that this might be a good initialization strategy for small data sets, as it would be computationally hard to associate a neuron to every data point since some datasets contain millions of datapoints.

## References

- Sanjeev Arora, Zhiyuan Li, and Kaifeng Lyu. Theoretical analysis of auto rate-tuning by batch normalization. In *International Conference on Learning Representations*, 2019. URL <https://openreview.net/forum?id=rkxQ-nA9FX>.
- Nils Bjorck, Carla P Gomes, Bart Selman, and Kilian Q Weinberger. Understanding batch normalization. In S. Bengio, H. Wallach, H. Larochelle, K. Grauman, N. Cesa-Bianchi, and R. Garnett, editors, *Advances in Neural Information Processing Systems*, volume 31. Curran Associates, Inc., 2018. URL <https://proceedings.neurips.cc/paper/2018/file/36072923bfc3cf47745d704feb489480-Paper.pdf>.
- Youngmin Cho and Lawrence Saul. Kernel methods for deep learning. In Y. Bengio, D. Schuurmans, J. Lafferty, C. Williams, and A. Culotta, editors, *Advances in Neural Information Processing Systems*, volume 22. Curran Associates, Inc., 2009. URL <https://proceedings.neurips.cc/paper/2009/file/5751ec3e9a4feab575962e78e006250d-Paper.pdf>.
- Hadi Daneshmand, Jonas Kohler, Francis Bach, Thomas Hofmann, and Aurelien Lucchi. Batch normalization provably avoids ranks collapse for randomly initialised deep networks. In H. Larochelle, M. Ranzato, R. Hadsell, M.F. Balcan, and H. Lin, editors, *Advances in Neural Information Processing Systems*, volume 33, page 18387–18398. Curran Associates, Inc., 2020. URL <https://proceedings.neurips.cc/paper/2020/file/d5ade38a2c9f6f073d69e1bc6b6e64c1-Paper.pdf>.
- Hadi Daneshmand, Amir Joudaki, and Francis Bach. Batch normalization orthogonalizes representations in deep random networks. In M. Ranzato, A. Beygelzimer, Y. Dauphin, P.S. Liang, and J. Wortman Vaughan, editors, *Advances in Neural Information Processing Systems*, volume 34, page 4896–4906. Curran Associates, Inc., 2021. URL <https://proceedings.neurips.cc/paper/2021/file/26cd8ecadce0d4efd6cc8a8725cbd1f8-Paper.pdf>.
- Soham De and Sam Smith. Batch normalization biases residual blocks towards the identity function in deep networks. *Advances in Neural Information Processing Systems*, 33:19964–19975, 2020.

- Sören Dittmer, Emily J. King, and Peter Maass. Singular values for relu layers. *IEEE Transactions on Neural Networks and Learning Systems*, 31(9):3594–3605, 2020. doi: 10.1109/TNNLS.2019.2945113.
- Jonathan Frankle, David J Schwab, and Ari S Morcos. Training batchnorm and only batchnorm: On the expressive power of random features in cnns. *arXiv preprint arXiv:2003.00152*, 2020.
- Yasutaka Furusho and Kazushi Ikeda. Theoretical analysis of skip connections and batch normalization from generalization and optimization perspectives. *APSIPA Transactions on Signal and Information Processing*, 9:e9, 2020.
- Kaiming He, Xiangyu Zhang, Shaoqing Ren, and Jian Sun. Delving deep into rectifiers: Surpassing human-level performance on imagenet classification. *CoRR*, abs/1502.01852, 2015. URL <http://arxiv.org/abs/1502.01852>.
- Kaiming He, Xiangyu Zhang, Shaoqing Ren, and Jian Sun. Deep residual learning for image recognition. In *2016 IEEE Conference on Computer Vision and Pattern Recognition (CVPR)*, pages 770–778, 2016. doi: 10.1109/CVPR.2016.90.
- Gao Huang, Zhuang Liu, Laurens Van Der Maaten, and Kilian Q. Weinberger. Densely connected convolutional networks. In *2017 IEEE Conference on Computer Vision and Pattern Recognition (CVPR)*, pages 2261–2269, 2017. doi: 10.1109/CVPR.2017.243.
- Sergey Ioffe and Christian Szegedy. Batch normalization: Accelerating deep network training by reducing internal covariate shift. In *International conference on machine learning*, pages 448–456. PMLR, 2015.
- Ryo Karakida, Shotaro Akaho, and Shun-ichi Amari. The normalization method for alleviating pathological sharpness in wide neural networks. In H. Wallach, H. Larochelle, A. Beygelzimer, F. d'Alché-Buc, E. Fox, and R. Garnett, editors, *Advances in Neural Information Processing Systems*, volume 32. Curran Associates, Inc., 2019. URL <https://proceedings.neurips.cc/paper/2019/file/9edda0fd4d983bf975935cfd492fd50b-Paper.pdf>.
- Xiang Li, Shuo Chen, Xiaolin Hu, and Jian Yang. Understanding the disharmony between dropout and batch normalization by variance shift. In *Proceedings of the IEEE/CVF conference on computer vision and pattern recognition*, pages 2682–2690, 2019.
- Ekdeep S Lubana, Robert Dick, and Hidenori Tanaka. Beyond batchnorm: Towards a unified understanding of normalization in deep learning. *Advances in Neural Information Processing Systems*, 34:4778–4791, 2021.
- Kaifeng Lyu, Zhiyuan Li, and Sanjeev Arora. Understanding the generalization benefit of normalization layers: Sharpness reduction. *arXiv preprint arXiv:2206.07085*, 2022.
- Shibani Santurkar, Dimitris Tsipras, Andrew Ilyas, and Aleksander Madry. How does batch normalization help optimization? In S. Bengio, H. Wallach, H. Larochelle, K. Grauman, N. Cesa-Bianchi, and R. Garnett, editors, *Advances in Neural Information Processing Systems*, volume 31. Curran Associates, Inc., 2018. URL <https://proceedings.neurips.cc/paper/2018/file/905056c1ac1dad141560467e0a99e1cf-Paper.pdf>.

Andrew M. Saxe, James L. McClelland, and Surya Ganguli. Exact solutions to the nonlinear dynamics of learning in deep linear neural network. In *In International Conference on Learning Representations*, 2014.

David Silver, Julian Schrittwieser, Karen Simonyan, Ioannis Antonoglou, Aja Huang, Arthur Guez, Thomas Hubert, Lucas Baker, Matthew Lai, Adrian Bolton, Yutian Chen, Timothy Lillicrap, Fan Hui, Laurent Sifre, George van den Driessche, Thore Graepel, and Demis Hassabis. Mastering the game of go without human knowledge. *Nature*, 550:354–, October 2017. URL <http://dx.doi.org/10.1038/nature24270>.

Jiaxi Wang, Ji Wu, and Lei Huang. Understanding the failure of batch normalization for transformers in nlp. *arXiv preprint arXiv:2210.05153*, 2022.

Greg Yang, Jeffrey Pennington, Vinay Rao, Jascha Sohl-Dickstein, and Samuel S Schoenholz. A mean field theory of batch normalization. *arXiv preprint arXiv:1902.08129*, 2019.

## Appendix A. Figures

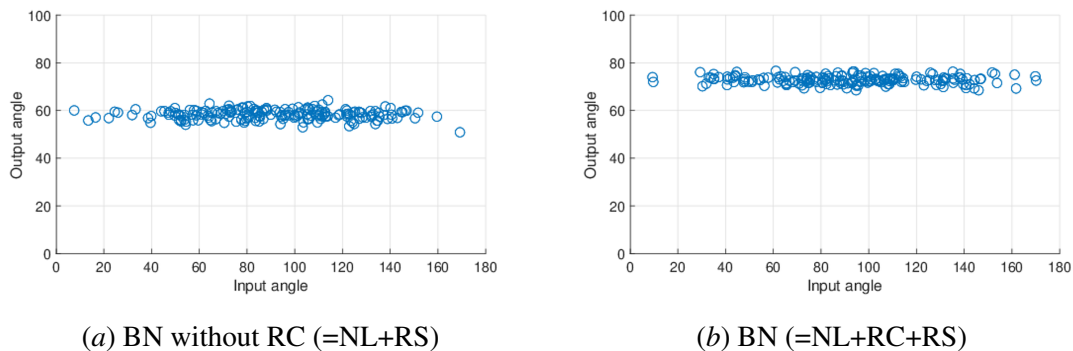


**Figure 5:** Effect of recentering on the angles between pairs of data points before and after the 30th layer of the neural network. If Batch Normalization without recentering is used, the output angles are approximately  $60^\circ$ . With recentering, the angles increase to approximately  $75^\circ$ .

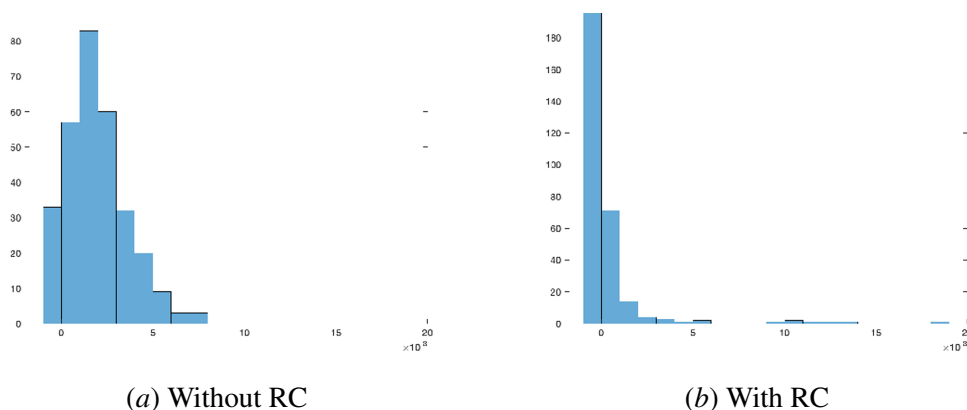


**Figure 6:** Histograms that represent the activity for a neuron in a network with and without RC. Without RC, some neurons exhibit neural activity like the one in Figure (a): the neuron has significant response for a large number of inputs. With RC, most of the neurons behave according to Figure (b): the neural response is negligible for most of the inputs.

## Appendix B. Proof of Theorem 3

**Proof** [Lemma 2] For  $\text{rank}(\text{ReLU}(W^{(r)}X^{(t)})) = t$ , the relation

$$\sum_{j=1}^t a_j \text{ReLU}(W^{(r)}\mathbf{x}_j) = \text{ReLU}(W^{(r)}\mathbf{x}_{t+1}) \quad (13)$$

either does not hold, in which case  $\text{rank}(\text{ReLU}(W^{(r+1)}X^{(t+1)})) = t + 1$  holds with probability 1 and equation (6) holds, or the relation holds for a *unique* set of  $\{a_i\}$ . Therefore, we are left with



treating the latter case. In that case, for the rank to remain  $t$ ,

$$\sum_{j=1}^{t+1} a_j \operatorname{ReLU}\left(W^{(r)}\mathbf{x}_j\right) = 0 \quad (14a)$$

has to hold with  $a_{t+1} := -1$ . Now, for equation (6) *not* to hold,

$$\sum_{j=1}^{t+1} a_j \operatorname{ReLU}\left(\mathbf{w}_{r+1}\mathbf{x}_j\right) = 0 \quad (14b)$$

has to hold with the same coefficients  $\{a_j\}$  as in equation (14a), namely,

$$\sum_{j=1}^{t+1} a_j \operatorname{ReLU}\left(W^{(r+1)}\mathbf{x}_j\right) = 0. \quad (14c)$$

We next prove that equation (14c) does not hold if, for some  $\ell \in [r]$  and  $i \in [t+1]$ ,

$$\operatorname{sign}\left(\mathbf{w}_{r+1}\mathbf{x}_i\right) \neq \operatorname{sign}\left(\mathbf{w}_\ell\mathbf{x}_i\right), \quad a_i \neq 0, \quad (15a)$$

$$\operatorname{sign}\left(\mathbf{w}_{r+1}\mathbf{x}_j\right) = \operatorname{sign}\left(\mathbf{w}_\ell\mathbf{x}_j\right) \quad \forall j \neq i. \quad (15b)$$

Furthermore, equation (15) for  $\ell \in [r]$ , such that  $\mathbf{w}_\ell \neq 0$ , holds with probability of at least  $\gamma\left(X^{(t+1)}\right)$ .

Take some  $\ell \in [r]$  for which  $\mathbf{w}_\ell \neq 0$  (there must exist such a row by the lemma assumption), and denote  $\mathcal{J}_\ell := \{j \in [t+1] : \mathbf{w}_\ell\mathbf{x}_j > 0, a_j \neq 0\}$ . Then, according to equation (14a),

$$\sum_{j=1}^{t+1} a_j \operatorname{ReLU}\left(\mathbf{w}_\ell\mathbf{x}_j\right) = \mathbf{w}_\ell \sum_{j \in \mathcal{J}_\ell} a_j \mathbf{x}_j = \mathbf{w}_\ell \mathbf{u} = 0, \quad (16)$$

with  $\mathbf{u} := \sum_{j \in \mathcal{J}} a_j \mathbf{x}_j$ , namely  $\mathbf{w}_\ell \perp \mathbf{u}^T$ .

If  $\mathbf{u} \neq 0$ , then  $\mathbf{w}_{r+1}\mathbf{u} \neq 0$  for  $\mathbf{w}_{r+1}$  in the equivalence class of  $\mathbf{w}_\ell$  (recall definition 1) up to measure zero, namely, with probability of at least  $\gamma\left(\tilde{X}^{(t+1)}\right)$ , where the columns of  $\tilde{X}^{(t+1)}$  are all the vectors in the set  $\{\mathbf{x}_j : a_j \neq 0, j \in [t+1]\}$ ; clearly,  $\gamma\left(\tilde{X}^{(t+1)}\right) \geq \gamma\left(X^{(t+1)}\right)$ .

If  $\mathbf{u} = 0$ , on the other hand, then

$$\sum_{j=1}^{t+1} a_j \operatorname{ReLU}\left(\mathbf{w}_{r+1}\mathbf{x}_j\right) = \mathbf{w}_{r+1}\left(\mathbf{u} \pm a_i\mathbf{x}_i\right) = \pm a_i \mathbf{w}_{r+1}\mathbf{x}_i \neq 0 \quad (17)$$

for  $\mathbf{w}_{r+1}$  that satisfies equation (15); we will show next that such  $\mathbf{w}_{r+1}$  constitute an equivalence class, meaning that equation (17) holds, again, with probability of at least  $\gamma\left(X^{(t+1)}\right)$ .

We are left with proving that the set of  $\mathbf{w}_{r+1}$  that satisfy equation (15) for a given  $\ell$  for which  $\mathbf{w}_\ell \neq 0$ , and some  $i$ , constitutes an equivalence class of non-zero volume. To that end, denote

$$i := \arg \min_{i \in [t+1]: a_i \neq 0} |\mathbf{w}_\ell\mathbf{x}_i|. \quad (18)$$

Then, for a sufficiently small  $\epsilon > 0$ ,

$$\left( \mathbf{w}_\ell - (1 + \epsilon) \frac{\mathbf{w}_\ell \mathbf{x}_i \mathbf{x}_i^T}{\|\mathbf{x}_i\|} \right) \mathbf{x}_i < 0 \quad (19)$$

$$\left( \mathbf{w}_\ell - (1 + \epsilon) \frac{\mathbf{w}_\ell \mathbf{x}_i \mathbf{x}_i^T}{\|\mathbf{x}_i\|} \right) \mathbf{x}_i > 0 \quad \forall j \in \{j \in [t+1] : j \neq i, a_j \neq 0\}, \quad (20)$$

since there are now collinear vectors in  $\{\mathbf{x}_j : j \in [t+1]\}$ . ■

**Proof** [Theorem 3] Denote the matrix composed of the first  $\ell$  columns of  $X$  by  $X^{(\ell)}$ . Denote further  $r_t := \min \{r \in \mathbb{N} : \text{ReLU}(W^{(r)} X^{(r)}) = t\}$  and  $y_t := r_t - r_{t-1}$  with  $r_0 := 0$ . Clearly,  $y = \sum_{t=1}^n y_t$ .

By the definition of  $r_t$ ,

$$\text{rank} \left( \text{ReLU} \left( W^{(r_t)} X^{(t)} \right) \right) = t. \quad (21)$$

Then, by lemma 2,

$$\text{rank} \left( \text{ReLU} \left( W^{(r_t+1)} X^{(t+1)} \right) \right) = t + 1 \quad (22)$$

with probability of at least  $\gamma(X^{(t+1)})$ . If

$$\text{rank} \left( \text{ReLU} \left( W^{(r_t+1)} X^{(t+1)} \right) \right) = t, \quad (23)$$

add another row; then,

$$\text{rank} \left( \text{ReLU} \left( W^{(r_t+2)} X^{(t+1)} \right) \right) = t + 1 \quad (24)$$

with probability of at least  $\gamma(X^{(t+1)})$ . Continue adding rows until the first  $r$  for which

$$\text{rank} \left( \text{ReLU} \left( W^{(r_t+r)} X^{(t+1)} \right) \right) = t + 1. \quad (25)$$

Identifying that  $y_t = r$  and noting that the cumulative distribution function (CDF) of  $r$  is majorized by that of a geometric distribution with success probability  $\gamma(X^{(t+1)})$ , yields

$$\mathbb{E}[y_t] \leq \frac{1}{\gamma(X^{(t+1)})}. \quad (26)$$

By noting that  $\gamma(X^{(t)})$  is a monotonically decreasing function in  $t$ , yields

$$\mathbb{E}[Y] = \sum_{t=1}^n \mathbb{E}[y_t] \leq \sum_{t=1}^n \frac{1}{\gamma(X^{(t+1)})} \leq \frac{n}{\gamma}. \quad (27)$$

This concludes the proof of item 1.

To prove item 2, note first that  $y_1, y_2, \dots, y_n$  are independent. Then,

$$\mathbb{P} \left( \text{rank}(\text{ReLU}(W^{(d)}X)) < n \right) \leq \mathbb{P} \left( y_1 + \dots + y_n > \frac{\alpha n}{\gamma} \right) \quad (28a)$$

$$\leq \min_{s>0} \left( \frac{\gamma \exp\{s\}}{1 - (1 - \gamma) \exp\{s\}} \right)^n \exp \left\{ -s \frac{\alpha n}{\gamma} \right\} \quad (28b)$$

$$= \exp \left\{ -n \left( \frac{\alpha}{\gamma} \log \frac{1}{\alpha} + \left( \frac{\alpha}{\gamma} - 1 \right) \log \frac{\alpha - \gamma}{1 - \gamma} \right) \right\} \quad (28c)$$

$$\leq \exp \{ -n (\alpha - 1 - \log \alpha) \} \quad (28d)$$

where equation (28a) follows from the definition of  $\{y_t\}$ ; equation (28b) follows from Chernoff's inequality by recalling that  $y_1, \dots, y_n$  are independent and that their (marginal) CDFs are majorized by that of a geometric distribution with success probability  $\gamma$ ; and equation (28d) follows from the monotonicity in  $\gamma$  of the expression in equation (28c). ■

### Appendix C. Proof of Theorem 10

By lemma 7, the sequence  $\{c(\mathbf{x}^{(t)}) : t \in \mathbb{N} \cup \{0\}\}$  is non-increasing. Assume that  $\mathbf{x}^{(0)}$  is not stable, i.e.,  $c(\mathbf{x}^{(0)}) > 3$ , as otherwise the result is trivially true. It suffices to prove that there exists a finite  $\tau \in \mathbb{N}$  such that  $\mathbf{x}^{(\tau)}$  is more clustered than  $\mathbf{x}^{(0)}$ . We start by proving this result in the case where the infinite sequence of transformations involves only positive transformations. Assume by contradiction that  $\mathbf{x}^{(t)}$  is not more clustered than  $\mathbf{x}^{(0)}$  for all  $t \in \mathbb{N}$ , i.e.,

$$c(\mathbf{x}^{(t)}) = c(\mathbf{x}^{(0)}) > 3 \quad \forall t \in \mathbb{N}. \quad (29)$$

Let  $n_t := \left| \left\{ i : x_i^{(t)} > 0 \right\} \right|$ , and define

$$\Delta_t := c_3(\mathbf{x}^{(t)}) - c_2(\mathbf{x}^{(t)}). \quad (30)$$

By the assumption in equation (29),

$$\Delta_{t_1} = \Delta_{t_2} := \Delta > 0, \quad n_{t_1} = n_{t_2} \geq 2, \quad (31)$$

for all  $t_1, t_2 \in \mathbb{N}$ . Thus, since, for all  $t \in \mathbb{N}$ ,  $x_i^{(t)} \geq 0$  for all  $i$ , we have

$$\bar{x}^{(t)} = \frac{1}{n} \sum_{i=1}^n x_i^{(t)} > \frac{\Delta}{n} \quad \forall t \in \mathbb{N}. \quad (32)$$

On the other hand, all the strictly positive entries  $x_i^{(t)}$  (which are  $n_t$ ) are all greater than the mean  $\bar{x}^{(t)}$ , as otherwise they would all go to zero at  $t + 1$ , in contradiction to equation (29). Therefore,

$$\bar{x}^{(t+1)} = \frac{1}{n} \sum_{i=1}^n x_i^{(t+1)} = \frac{1}{n} \sum_{i=1}^n \text{ReLU} \left( x_i^{(t)} - \bar{x}^{(t)} \right) = \bar{x}^{(t)} - \frac{n_t}{n} \bar{x}^{(t)} = \left( 1 - \frac{n_t}{n} \right) \bar{x}^{(t)}, \quad (33)$$

from which it follows that  $\lim_{t \rightarrow \infty} \bar{x}^{(t)} = 0$  since  $n_t \geq 2$  for all  $t \in \mathbb{N}$ . This contradicts equation (32), thus proving the result.

The case of a *finite* number of negative transformations simply follows from the previous case, by repeating the previous proof from layer  $t \in \mathbb{N}$  that corresponds to the last negative transformation in lieu of layer 0.

Finally, consider the case where there are an infinite number of negative transformations, and assume again equation (29) by contradiction. Consider any two steps  $t_1$  and  $t_2$  of the sequence such that a negative transformation occurs at  $t_1$  and  $t_2$ , and only positive transformations occur between these two steps, viz.

$$\mathbf{x}^{(t_1)} = \text{ReLU}(-\mathbf{x}^{(t_1-1)} + \bar{x}^{(t_1-1)}), \quad (34a)$$

$$\mathbf{x}^{(t)} = \text{ReLU}(\mathbf{x}^{(t-1)} - \bar{x}^{(t-1)}), \quad t_1 < t < t_2. \quad (34b)$$

$$\mathbf{x}^{(t_2)} = \text{ReLU}(-\mathbf{x}^{(t_2-1)} + \bar{x}^{(t_2-1)}), \quad (34c)$$

We now show that this sequence of transformations decreases the mean, i.e.,  $\bar{x}^{(t_2)} < \bar{x}^{(t_1-1)}$ . To that end, denote  $x_{\max}^{(t)} := \max \mathbf{x}^{(t)}$ , and  $I_t := \{i : x_i^{(t)} < x_{\max}^{(t)}\}$ . Then,

$$\bar{x}^{(t_2)} = \frac{1}{n} \sum_{i=1}^n x_i^{(t_2)} \quad (35a)$$

$$= \frac{1}{n} \sum_{i \in I_{t_2-1}} \left( -x_i^{(t_2-1)} + \bar{x}^{(t_2-1)} \right) \quad (35b)$$

$$= \left( 1 - \frac{n_{t_2}}{n} \right) \left( x_{\max}^{(t_2-1)} - \bar{x}^{(t_2-1)} \right) \quad (35c)$$

$$< \left( 1 - \frac{n_{t_2}}{n} \right) \left( x_{\max}^{(t_1)} - \bar{x}^{(t_1)} \right) \quad (35d)$$

$$= \left( 1 - \frac{n_{t_2}}{n} \right) \left( \bar{x}^{(t_1-1)} - \bar{x}^{(t_1)} \right) \quad (35e)$$

$$< \left( 1 - \frac{2}{n} \right) \bar{x}^{(t_1-1)} \quad (35f)$$

where equation (35b) follows from equation (34c) and the assumption in equation (29), which suggests that exactly one of the clusters will be nullified by the ReLU activation, as otherwise  $c(\mathbf{x}^{(t_2-1)}) = 1$  or  $c(\mathbf{x}^{(t_2)}) < c(\mathbf{x}^{(t_2-1)})$ , in contradiction to equation (29); equation (35c) follows from the definition of  $n_{t_2}$ ,  $x_{\max}^{(t_2-1)}$ , and  $\bar{x}^{(t_2-1)}$ ; equation (35d) follows from equation (33); equation (35e) follows from equation (34a) by noting that  $x_{\max}^{(t_1)} = \bar{x}^{(t_1-1)}$ ; and equation (35f) holds since  $\bar{x}^{(t_1)} > 0$  and  $n_{t_2} \geq 2$  by equation (31).

Hence, a sequence of negative transformations, with each pair of consecutive such transformations possibly separated by several intermediate positive transformations, contracts the vector mean, meaning that  $\lim_{t \rightarrow \infty} \bar{x}^{(t)} = 0$ . However, since equation (32) still holds for this case, we again reach a contradiction, and the theorem is proved.

## Appendix D. Proof of Theorem 11 for two clusters

Due to Theorem 10, there exists a  $t_0 \geq 1$  such that for every  $t \geq t_0$ , every row/neuron of  $X^{(t)}$  is a vector composed of at most 3 clusters. To improve the readability and ease of understanding of

the proof, we first prove the theorem neglecting the presence of three-cluster rows. This is because the main ideas are already present in this simpler case, and three-cluster rows only introduce some unenlightening technicalities to the proof. We address these technicalities in Appendix E, where we prove that three-cluster rows do not invalidate the result.

To prove the first point of the theorem, notice that, due to the fact that the components of each row of  $X^{(t)}$  are ordered, each cluster is composed of consecutive elements. Hence, the first and the last element of each row are always in two different clusters: either the first element is zero and the last is strictly positive, or vice versa. Hence, the product of these two elements is always zero, and therefore  $\langle \mathbf{x}_1^{(t)}, \mathbf{x}_n^{(t)} \rangle = 0$ .

To prove the second part of the theorem, consider any row of  $X^{(t)}$  that is composed of two clusters, and recall that one of the two clusters must be at zero, and the other one at a positive coordinate. We will refer to those clusters as the *zero cluster* and the *positive cluster* respectively. After  $T$  additional layers, the selected row undergoes any possible sequence of  $T$  positive and/or negative transformations, generating a total of  $2^T$  rows in the matrix  $X^{(t+T)}$ . We want to study the contribution of these  $2^T$  rows to the inner product between any two columns of  $X^{(t+T)}$ .

Let  $i, j \in \{2, \dots, n-1\}$  be the two selected columns. First of all, notice that the  $2^T$  rows generated by a given row at layer  $t$ , will contribute to the inner product between  $i$  and  $j$  only if elements  $i$  and  $j$  of the given row are in the same cluster at layer  $t$ ; otherwise, one of the two elements will necessarily be zero. Furthermore, of the corresponding  $2^T$  rows at layer  $t+T$ , those that contribute to the inner product are only the ones in which the cluster containing  $i$  and  $j$  is the positive one. Hence, the given neuron at layer  $t$  has to undergo a sequence of positive/negative transformations in such a way that after  $T$  layers, the cluster containing  $i$  and  $j$  is the positive one.

Keeping all of this in mind, the next step is to study how a two-cluster vector changes after a given sequence of  $T$  positive/negative transformations. Consider any vector of  $n$  elements composed of two clusters: one cluster is at coordinate 0 (the zero cluster) and it is made of  $n_0$  elements, while the second cluster (the positive cluster) is at coordinate  $c > 0$  and it is made of  $n - n_0$  elements. From now on, we say that such a vector has *composition*  $(n_0, n - n_0)$ . After one positive transformation, the zero cluster remains unchanged, while the coordinate of the positive cluster becomes

$$c' = c - \frac{n - n_0}{n}c = \frac{n_0}{n}c. \quad (36)$$

After a negative transformation, instead, the zero and positive cluster switch roles: the positive cluster goes at coordinate 0 and becomes the new zero cluster, while the old zero cluster becomes the new positive cluster. Thus, the new vector has composition  $(n - n_0, n_0)$ , and the new coordinate of the positive cluster is equal to

$$c' = \frac{n - n_0}{n}c. \quad (37)$$

See Figure 7 for a visual representation of this process. Thus, one can see that what really determines the new coordinate of the positive cluster after one transformation is the number of points in the zero cluster *after* the transformation: in the first case, the number of points is  $n_0$ , while in the second case it is  $n - n_0$ . After  $T$  transformations, in which for  $k$  times the zero cluster contains  $n_0$  points, and for  $T - k$  times it contains  $n - n_0$  points, the final coordinate of the positive cluster is

$$c' = \left(\frac{n_0}{n}\right)^k \left(\frac{n - n_0}{n}\right)^{T-k} c. \quad (38)$$

Hence, for a row  $\mathbf{x}_\ell^{(t)}$  at layer  $t$  in which elements  $i$  and  $j$  are in the same cluster with  $n_\ell$  elements, all the neurons generated from it after a sequence of  $T$  transformations in which their cluster ends in a positive coordinate  $c$ , contributes to the inner product, with a value equal to  $c^2$ . Following equation (38), the total contribution is

$$C_\ell = \sum_{k=0}^{T-1} \binom{T-1}{k} \left(\frac{n-n_\ell}{n}\right)^{2(T-k)} \left(\frac{n_\ell}{n}\right)^{2k} c_\ell^2 \quad (39)$$

$$= c_\ell^2 \left(\frac{n-n_\ell}{n}\right)^2 \left\{ \left(\frac{n-n_\ell}{n}\right)^2 + \left(\frac{n_\ell}{n}\right)^2 \right\}^{T-1} \quad (40)$$

where  $c_\ell$  is the coordinate of the positive cluster of  $\mathbf{x}_\ell^{(t)}$ . Note that the leading term  $\left(\frac{n-n_\ell}{n}\right)^2$  and the  $T-1$  exponent appear because, after any sequence of  $T-1$  transformations, the  $T$ -th and last one is fixed, since the cluster containing elements  $i$  and  $j$  must end in a positive coordinate. As one can see, all contributions decrease exponentially with  $T$ , and the exponent depends on the composition of the two clusters. The compositions that dominate are the most unbalanced ones: those with one point in one cluster and  $n-1$  points in the other. Thus, we can limit our attention to the leaves belonging to the set

$$L_{i,j}^{(t)} = \{\ell : \mathbf{x}_\ell^{(t)} \text{ has two clusters of composition } (1, n-1) \text{ or } (n-1, 1) \\ \text{with elements } i, j \text{ in the same cluster}\} \quad (41)$$

since, asymptotically as  $T$  goes to infinity, these are the only ones that contribute to the inner product. Note that for any pair  $i, j$ , such unbalanced configurations always exist, since there is always a path of positive/negative transformations that leads to them. Hence, the set  $L_{i,j}^{(t)}$  is not empty. Furthermore, if a cluster contains  $n-1$  elements, then these elements must be either  $\{2, \dots, n\}$  or  $\{1, \dots, n-1\}$ . Hence, all elements in  $\{2, \dots, n-2\}$  must belong to the same cluster. Thus, the set defined in equation (41) contains the same neurons for any pair  $i, j \in \{2, \dots, n-1\}$ , and we can define a single set independent of  $i, j$ :

$$L^{(t)} = \{\ell : \mathbf{x}_\ell^{(t)} \text{ has two clusters of composition } (1, n-1) \text{ or } (n-1, 1)\} \quad (42)$$

so that  $L_{i,j}^{(t)} = L^{(t)}$  for every  $i, j \in \{2, \dots, n\}$ . The total contribution of the clusters that belong to  $L^{(t)}$  amounts to

$$\sum_{\ell \in L^{(t)}} C_\ell = \frac{1}{n^2} \left\{ \left(\frac{1}{n}\right)^2 + \left(\frac{n-1}{n}\right)^2 \right\}^{T-1} \sum_{\ell \in L^{(t)}} c_\ell^2 \quad (43)$$

which is independent of the actual choice of  $i$  and  $j$ .

Regarding the norm of a single element  $i$ , the same reasoning applies, with the difference that the rows that contribute to it are all those in which  $i$  is in the positive cluster. Again, the dominant configurations are the most unbalanced ones, and since  $i$  and  $j$  are not extreme points, the dominant configurations that contribute to the norms  $\|\mathbf{x}_i^{(t+T)}\|$  and  $\|\mathbf{x}_j^{(t+T)}\|$  are exactly the same

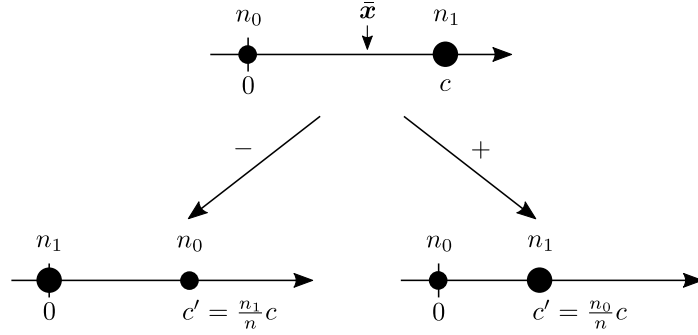


**Figure 7:** Example of evolution of stable configurations with two clusters. The number of points in the two clusters are denoted by  $n_0$  and  $n_1$ .

that contribute to  $\langle \mathbf{x}_i^{(t+T)}, \mathbf{x}_j^{(t+T)} \rangle$ , i.e., those in  $L^{(t)}$ . Thus, we have

$$\begin{aligned} & \lim_{T \rightarrow \infty} \frac{\langle \mathbf{x}_i^{(t+T)}, \mathbf{x}_j^{(t+T)} \rangle}{\|\mathbf{x}_i^{(t+T)}\| \|\mathbf{x}_j^{(t+T)}\|} \\ &= \lim_{T \rightarrow \infty} \frac{\frac{1}{n^2} \left\{ \left(\frac{1}{n}\right)^2 + \left(\frac{n-1}{n}\right)^2 \right\}^{T-1} \sum_{\ell \in L^{(t)}} c_\ell^2 + o\left(\left(\frac{1}{n}\right)^2 + \left(\frac{n-1}{n}\right)^2\right)^T}{\frac{1}{n^2} \left\{ \left(\frac{1}{n}\right)^2 + \left(\frac{n-1}{n}\right)^2 \right\}^{T-1} \sum_{\ell \in L^{(t)}} c_\ell^2 + o\left(\left(\frac{1}{n}\right)^2 + \left(\frac{n-1}{n}\right)^2\right)^T} = 1. \end{aligned} \quad (44)$$

where  $\frac{o\left(\left(\frac{1}{n}\right)^2 + \left(\frac{n-1}{n}\right)^2\right)^T}{\left(\left(\frac{1}{n}\right)^2 + \left(\frac{n-1}{n}\right)^2\right)^T} \rightarrow 0$  as  $T \rightarrow \infty$ .

As shown in Appendix A, the contribution of three-cluster configurations does not change the validity of equation (44), so the second part of the theorem is proved.

To prove the third part, recall that, from the previous discussion, we showed that, asymptotically as  $T \rightarrow \infty$ , the norm of any vector  $\mathbf{x}_i^{(t+T)}$  for  $i \in \{2, \dots, n-1\}$  is equal to, following equation (43),

$$\|\mathbf{x}_i^{(t+T)}\|^2 \simeq \frac{1}{n^2} \left\{ \left(\frac{1}{n}\right)^2 + \left(\frac{n-1}{n}\right)^2 \right\}^{T-1} \sum_{\ell \in L^{(t)}} c_\ell^2. \quad (45)$$

Next, notice that the vectors belonging to  $L^{(t)}$  can have two different compositions, namely  $(1, n-1)$  and  $(n-1, 1)$ . While the rows with these two compositions have the same contribution to the norm of a vector with index between 2 and  $n-1$ , this is not true anymore for the extreme vectors  $\mathbf{x}_1^{(t+T)}$  and  $\mathbf{x}_n^{(t+T)}$ . In fact, for a row at layer  $t$  with composition  $(1, n-1)$ , out of the  $2^T$  rows generated by it at layer  $t+T$ , those that contribute to  $\|\mathbf{x}_1^{(t+T)}\|$  and those that contribute to  $\|\mathbf{x}_i^{(t+T)}\|$  for  $i \in \{2, \dots, n-1\}$  are complementary sets. If instead the starting configuration is  $(n-1, 1)$ , then the rows that contribute to the two norms are exactly the same, since points 1 and  $i$  belong to the same cluster. A similar reasoning applies also to  $\|\mathbf{x}_n^{(t+T)}\|$ .

Let us call  $L_1^{(t)}$  the set of rows at layer  $t$  with composition  $(1, n-1)$ , and  $L_2^{(t)}$  those with composition  $(n-1, 1)$ . Then,  $L^{(t)} = L_1^{(t)} \cup L_2^{(t)}$ . Following equation (40), the total contribution to

$\|\mathbf{x}_1^{(t+T)}\|$  of the rows in  $L^{(t)}$  is

$$\|\mathbf{x}_1^{(t+T)}\|^2 \simeq \left\{ \left( \frac{1}{n} \right)^2 + \left( \frac{n-1}{n} \right)^2 \right\}^{T-1} \left( \left( \frac{n-1}{n} \right)^2 \sum_{\ell \in L_1^{(t)}} c_\ell^2 + \left( \frac{1}{n} \right)^2 \sum_{\ell \in L_2^{(t)}} c_\ell^2 \right). \quad (46)$$

Similarly, one has

$$\|\mathbf{x}_n^{(t+T)}\|^2 \simeq \left\{ \left( \frac{1}{n} \right)^2 + \left( \frac{n-1}{n} \right)^2 \right\}^{T-1} \left( \left( \frac{1}{n} \right)^2 \sum_{\ell \in L_1^{(t)}} c_\ell^2 + \left( \frac{n-1}{n} \right)^2 \sum_{\ell \in L_2^{(t)}} c_\ell^2 \right). \quad (47)$$

Hence, we can write

$$\frac{\|\mathbf{x}_i^{(t+T)}\|^2}{\|\mathbf{x}_1^{(t+T)}\|^2} \simeq \frac{\left( \frac{1}{n} \right)^2 \sum_{\ell \in L^{(t)}} c_\ell^2}{\left( \frac{n-1}{n} \right)^2 \sum_{\ell \in L_1^{(t)}} c_\ell^2 + \left( \frac{1}{n} \right)^2 \sum_{\ell \in L_2^{(t)}} c_\ell^2} \quad (48)$$

$$= \frac{1 + \frac{\sum_{\ell \in L_2^{(t)}} c_\ell^2}{\sum_{\ell \in L_1^{(t)}} c_\ell^2}}{(n-1)^2 + \frac{\sum_{\ell \in L_2^{(t)}} c_\ell^2}{\sum_{\ell \in L_1^{(t)}} c_\ell^2}} \quad (49)$$

and, similarly,

$$\frac{\|\mathbf{x}_i^{(t+T)}\|^2}{\|\mathbf{x}_n^{(t+T)}\|^2} \simeq \frac{1 + \frac{\sum_{\ell \in L_1^{(t)}} c_\ell^2}{\sum_{\ell \in L_2^{(t)}} c_\ell^2}}{(n-1)^2 + \frac{\sum_{\ell \in L_1^{(t)}} c_\ell^2}{\sum_{\ell \in L_2^{(t)}} c_\ell^2}}. \quad (50)$$

Therefore, if  $\frac{\sum_{\ell \in L_2^{(t)}} c_\ell^2}{\sum_{\ell \in L_1^{(t)}} c_\ell^2} \leq 1$ , then

$$\frac{\|\mathbf{x}_i^{(t+T)}\|^2}{\|\mathbf{x}_1^{(t+T)}\|^2} \lesssim \frac{2}{(n-1)^2}. \quad (51)$$

If instead  $\frac{\sum_{\ell \in L_2^{(t)}} c_\ell^2}{\sum_{\ell \in L_1^{(t)}} c_\ell^2} > 1$ , then

$$\frac{\|\mathbf{x}_i^{(t+T)}\|^2}{\|\mathbf{x}_n^{(t+T)}\|^2} \lesssim \frac{2}{(n-1)^2}. \quad (52)$$

As shown in Appendix A, the contribution of three-cluster configurations makes the bounds in equation (51) and equation (52) larger (as in the statement of the theorem), but does not change the general validity of the result.



The proof of the fourth part of the theorem is similar to the third. In fact, we can write

$$\langle \mathbf{x}_i^{(t+T)}, \mathbf{x}_1^{(t+T)} \rangle \simeq \left(\frac{1}{n}\right)^2 \left\{ \left(\frac{1}{n}\right)^2 + \left(\frac{n-1}{n}\right)^2 \right\}^{T-1} \sum_{\ell \in L_2^{(t)}} c_\ell^2 \quad (53)$$

and

$$\langle \mathbf{x}_i^{(t+T)}, \mathbf{x}_n^{(t+T)} \rangle \simeq \left(\frac{1}{n}\right)^2 \left\{ \left(\frac{1}{n}\right)^2 + \left(\frac{n-1}{n}\right)^2 \right\}^{T-1} \sum_{\ell \in L_1^{(t)}} c_\ell^2 \quad (54)$$

Hence, using also equation (46), equation (47) and equation (45), one has

$$\angle \left( \mathbf{x}_i^{(t+T)}, \mathbf{x}_1^{(t+T)} \right) = \arccos \frac{\langle \mathbf{x}_i^{(t+T)}, \mathbf{x}_1^{(t+T)} \rangle}{\|\mathbf{x}_i^{(t+T)}\| \|\mathbf{x}_1^{(t+T)}\|} \quad (55)$$

$$\simeq \arccos \frac{\sum_{\ell \in L_2^{(t)}} c_\ell^2}{\sqrt{\sum_{\ell \in L_1^{(t)}} c_\ell^2 + \sum_{\ell \in L_2^{(t)}} c_\ell^2} \sqrt{(n-1)^2 \sum_{\ell \in L_1^{(t)}} c_\ell^2 + \sum_{\ell \in L_2^{(t)}} c_\ell^2}} \quad (56)$$

$$= \arccos \frac{1}{\sqrt{\frac{\sum_{\ell \in L_1^{(t)}} c_\ell^2}{\sum_{\ell \in L_2^{(t)}} c_\ell^2} + 1} \sqrt{(n-1)^2 \frac{\sum_{\ell \in L_1^{(t)}} c_\ell^2}{\sum_{\ell \in L_2^{(t)}} c_\ell^2} + 1}} \quad (57)$$

and similarly,

$$\angle \left( \mathbf{x}_i^{(t+T)}, \mathbf{x}_n^{(t+T)} \right) \simeq \arccos \frac{1}{\sqrt{\frac{\sum_{\ell \in L_2^{(t)}} c_\ell^2}{\sum_{\ell \in L_1^{(t)}} c_\ell^2} + 1} \sqrt{(n-1)^2 \frac{\sum_{\ell \in L_2^{(t)}} c_\ell^2}{\sum_{\ell \in L_1^{(t)}} c_\ell^2} + 1}}. \quad (58)$$

Therefore, if  $\frac{\sum_{\ell \in L_2^{(t)}} c_\ell^2}{\sum_{\ell \in L_1^{(t)}} c_\ell^2} \leq 1$ , then

$$\angle \left( \mathbf{x}_i^{(t+T)}, \mathbf{x}_1^{(t+T)} \right) \gtrsim \arccos \frac{1}{\sqrt{2}(n-1)} \geq \frac{\pi}{2} - \frac{\pi}{2\sqrt{2}(n-1)}. \quad (59)$$

Otherwise,

$$\angle \left( \mathbf{x}_i^{(t+T)}, \mathbf{x}_n^{(t+T)} \right) \gtrsim \frac{\pi}{2} - \frac{\pi}{2\sqrt{2}(n-1)}. \quad (60)$$

Once again, three-cluster configurations slightly change the value of the bound, as shown in Appendix A.

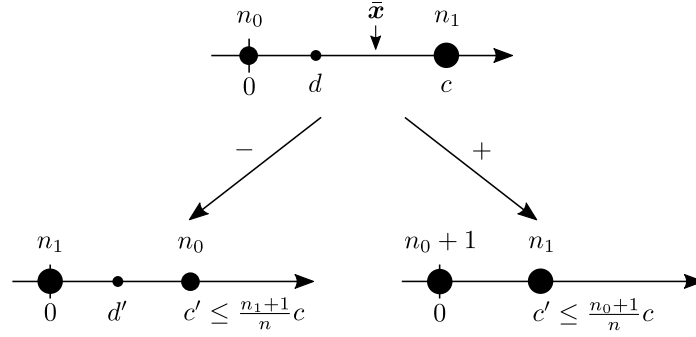


**Figure 8:** Example of evolution of stable configurations with three clusters. Notice that, at every step, a three-cluster neuron always generates one three-cluster neuron and one two-cluster neuron.

## Appendix E. Contribution of three-cluster configurations to Theorem 11

In Theorem 11, rows at layer  $t$  which are composed of three clusters must also be taken into account. To complete the proof of the second point of the theorem, we now show that their total contribution to the numerator and the denominator in equation (11) are asymptotically equal, and therefore equation (44) still holds in the general case.

First of all, for the same reasoning as in the two-cluster case, a three-cluster row at layer  $t$  will have a non-negligible contribution at layer  $t+T$  only if at some point during the process between layer  $t$  and layer  $t+T$ , it generates two-cluster rows with composition  $(1, n-1)$  or  $(n-1, 1)$ ; otherwise, its contribution will be negligible compared to the contribution of the two-cluster configurations belonging to  $L^{(t)}$ . Such three-cluster rows must have composition  $(1, 1, n-2)$  or  $(n-2, 1, 1)$  — the cluster in the middle must contain only one element by construction. Furthermore, once again by construction, a three-cluster row at layer  $t$  generates  $2^T$  rows at layer  $T$ , out of which exactly one is composed of three-clusters row, and the other  $2^T - 1$  are two-cluster ones.

The contribution of the single three-cluster row is negligible, and this can be proved even by using very loose bounds. In fact, for any three-cluster configuration, let  $c$  be the coordinate of the largest cluster. Then, after one layer, both the new coordinates of the middle and the largest clusters can be upper bounded by  $\frac{n-1}{n}c$ . Thus, after  $T$  layers, the final coordinates are upper bounded by  $\left(\frac{n-1}{n}\right)^T c$ . Hence, its contribution to the inner products or to the norms will be at most  $\left(\frac{n-1}{n}\right)^{2T} c^2$ , which has a negligible exponent compared to equation (40).

Regarding the contribution of the other rows, first notice that, if the elements  $i$  and  $j$  are both in the largest cluster at layer  $t$ , they will remain paired (i.e., in the same cluster) in all the rows generated at layer  $t+T$ . Thus, as before, the contribution of the rows will be exactly the same in the inner product at the numerator of equation (11), and in the product of the norms in the denominator. The remaining case is that in which one element is in the middle cluster, and the other is in the largest cluster. Notice that, at each step, a three-cluster row generates two rows: one has a three-cluster configuration, while the other one has two clusters, with composition  $(n-1, 1)$  or  $(2, n-2)$  (see Figure 8 for a visual example). Thus, at layer  $t+T$ , the two-cluster rows have composition  $(n-1, 1)$ ,  $(1, n-1)$ ,  $(2, n-2)$  or  $(n-2, 2)$ . The rows with compositions  $(n-1, 1)$  or  $(1, n-1)$  give, once again, the same contribution to the numerator and the denominator of equation (11). Instead, those with composition  $(2, n-2)$  or  $(n-2, 2)$  give different contributions: they give zero contribution to the inner product, since the two elements under consideration belong to different clusters, but they

contribute to each of the norms. However, asymptotically their total contribution is negligible. In fact, the contribution to both  $\|\mathbf{x}_i^{(t+T)}\|^2$  and  $\|\mathbf{x}_j^{(t+T)}\|^2$  can be upper bounded, thanks to equation (40), by

$$c^2 \left(\frac{n-2}{n}\right)^2 \left\{ \left(\frac{n-1}{n}\right)^2 \left[ \left(\frac{2}{n}\right)^2 + \left(\frac{n-2}{n}\right)^2 \right]^{T-2} + \left(\frac{n-1}{n}\right)^4 \left[ \left(\frac{2}{n}\right)^2 + \left(\frac{n-2}{n}\right)^2 \right]^{T-3} + \dots + \left(\frac{n-1}{n}\right)^{2(T-1)} \right\} \quad (61)$$

$$\leq c^2 \left(\frac{n-2}{n}\right)^2 \left(\frac{n^2-2n+1}{2n-7}\right) \left(\frac{n-1}{n}\right)^{2(T-1)} \quad (62)$$

which has a negligible exponent with respect to equation (40). Hence, we proved that three-cluster configurations do not affect the validity of equation (44), and the second part of the theorem is proved.

For the third part of the theorem, the three-cluster configurations that contribute to the norms are again only those of the form  $(1, 1, n-2)$  or  $(n-2, 1, 1)$ , since those are the only non-negligible ones. First, let us consider a three-cluster row at layer  $t$  of composition  $(1, 1, n-2)$  and an element  $i \in \{3, n-2\}$ . We want to study the cumulative contribution at layer  $t+T$  of all the rows generated by the selected one at layer  $t$ . Notice that, at layer  $t+T-1$ , one generated row is of composition  $(1, 1, n-2)$ , and the others have composition  $(1, n-1)$  or  $(2, n-2)$ . The contribution of the single three-cluster row is negligible, as we already discussed above. For a row of composition  $(1, n-1)$ , let  $c(T)$  be the value of the coordinate of the positive cluster at layer  $t+T-1$  (which depends exponentially on  $T$ ). Of its two children at layer  $t+T$ , one contributes to the norm of  $\mathbf{x}_i^{(t+T)}$  and  $\mathbf{x}_n^{(t+T)}$  an amount equal to  $\frac{1}{n^2}c^2(T)$ , and the other one to the norm of  $\mathbf{x}_1^{(t+T)}$  an amount equal to  $\left(\frac{n-1}{n}\right)^2 c^2(T)$ . Similarly, for a row of composition  $(2, n-2)$ , one contributes to the norm of  $\mathbf{x}_i^{(t+T)}$  and  $\mathbf{x}_n^{(t+T)}$  an amount equal to  $\frac{4}{n^2}c^2(T)$ , and the other one to the norm of  $\mathbf{x}_1^{(t+T)}$  an amount equal to  $\left(\frac{n-2}{n}\right)^2 c^2(T)$ . A similar reasoning can be applied to three-cluster neurons at layer  $t$  with composition  $(n-2, 1, 1)$ . Putting everything together, define  $A(T)$  to be the sum of the squares of the positive coordinates of all rows of composition  $(1, n-1)$  at layer  $t+T-1$ , let  $B(T)$  be the same for rows of composition  $(n-1, 1)$ ,  $C(T)$  for rows of composition  $(2, n-2)$ , and  $D(T)$  for rows of composition  $(n-2, 2)$ . Then, we have:

$$\|\mathbf{x}_i^{(t+T)}\|^2 \simeq \frac{1}{n^2}A(T) + \frac{1}{n^2}B(T) + \frac{4}{n^2}C(T) + \frac{4}{n^2}D(T) \quad (63)$$

$$\|\mathbf{x}_1^{(t+T)}\|^2 \simeq \left(\frac{n-1}{n}\right)^2 A(T) + \frac{1}{n^2}B(T) + \left(\frac{n-2}{n}\right)^2 C(T) + \frac{4}{n^2}D(T) \quad (64)$$

$$\|\mathbf{x}_n^{(t+T)}\|^2 \simeq \frac{1}{n^2}A(T) + \left(\frac{n-1}{n}\right)^2 B(T) + \frac{4}{n^2}C(T) + \left(\frac{n-2}{n}\right)^2 D(T) \quad (65)$$

from which it follows that

$$\frac{\|\mathbf{x}_i^{(t+T)}\|^2}{\|\mathbf{x}_1^{(t+T)}\|^2} \simeq \frac{A(T) + B(T) + 4C(T) + 4D(T)}{(n-1)^2A(T) + B(T) + (n-2)^2C(T) + 4D(T)} \quad (66)$$

$$\leq \frac{4(A(T) + C(T)) + 4(B(T) + D(T))}{(n-2)^2(A(T) + C(T)) + (B(T) + D(T))} \quad (67)$$

$$= \frac{4 + 4\frac{B(T)+D(T)}{A(T)+C(T)}}{(n-2)^2 + \frac{B(T)+D(T)}{A(T)+C(T)}} \quad (68)$$

and

$$\frac{\|\mathbf{x}_i^{(t+T)}\|^2}{\|\mathbf{x}_n^{(t+T)}\|^2} \simeq \frac{A(T) + B(T) + 4C(T) + 4D(T)}{A(T) + (n-1)^2B(T) + 4C(T) + (n-2)^2D(T)} \quad (69)$$

$$\leq \frac{4(A(T) + C(T)) + 4(B(T) + D(T))}{(n-2)^2(B(T) + D(T)) + (A(T) + C(T))} \quad (70)$$

$$= \frac{4 + 4\frac{A(T)+C(T)}{B(T)+D(T)}}{(n-2)^2 + \frac{A(T)+C(T)}{B(T)+D(T)}} \quad (71)$$

since  $A(T), B(T), C(T)$  and  $D(T)$  are all positive for every  $T \geq 1$ . Furthermore,  $\frac{A(T)+C(T)}{B(T)+D(T)}$  converges to a constant as  $T \rightarrow \infty$ . Hence, for every  $T$  larger than a certain value, either  $\frac{A(T)+C(T)}{B(T)+D(T)} \leq 1$  or  $\frac{B(T)+D(T)}{A(T)+C(T)} \leq 1$ . From this, it follows that either

$$\lim_{t \rightarrow \infty} \frac{\|\mathbf{x}_i^{(t)}\|^2}{\|\mathbf{x}_1^{(t)}\|^2} \leq \frac{8}{(n-2)^2} \quad (72)$$

or

$$\lim_{t \rightarrow \infty} \frac{\|\mathbf{x}_i^{(t)}\|^2}{\|\mathbf{x}_n^{(t)}\|^2} \leq \frac{8}{(n-2)^2} \quad (73)$$

which proves the theorem, for the case of  $i \in \{3, \dots, n-2\}$ . To complete the proof of part three, the case of points  $i = 2$  and  $i = n-1$  must be considered. We analyze the case  $i = 2$ , since the other case follows in the same way by symmetry. Let  $\ell$  be any three-cluster row at layer  $t$  with composition  $(1, 1, n-2)$ . During the next  $T$  layers, point  $i = 2$  will get paired with point 1 only in  $(2, n-2)$  cluster configurations, whose contribution compared to  $(1, n-1)$  ones is negligible, per equation (62). The only other two-cluster configurations generated during the process are  $(1, n-1)$  ones, in which point 2 is always paired with point  $n$ . Thus, for those clusters, due to equation (40), the final contribution at layer  $t+T$  will be of the form  $\frac{1}{n^2}e_\ell(T)$  for the norms  $\|\mathbf{x}_2^{(t+T)}\|^2$  and  $\|\mathbf{x}_n^{(t+T)}\|^2$ , and of the form  $\left(\frac{n-1}{n}\right)^2 e_\ell(T)$  for  $\|\mathbf{x}_1^{(t+T)}\|^2$ , where  $e_\ell(T)$  is an exponentially-decaying function of  $T$ , whose exponent can be at most  $\left\{\left(\frac{1}{n}\right)^2 + \left(\frac{n-1}{n}\right)^2\right\}^{T-1}$ . Denote by  $C(T)$  the cumulative exponent for all  $(1, 1, n-2)$  rows at layer  $t$ , i.e.,  $C(T) = \sum_\ell e_\ell(T)$ , where the sum is over all three-cluster rows at layer  $t$  with composition  $(1, 1, n-2)$ . On the contrary, for three-cluster rows

with composition  $(n - 2, 1, 1)$ , point 2 is always paired with point 1. Hence, if  $\ell$  is such a row, the final contribution at layer  $t + T$  will be of the form  $\frac{1}{n^2} e_\ell(T)$  for the norms  $\|\mathbf{x}_1^{(t+T)}\|^2$  and  $\|\mathbf{x}_2^{(t+T)}\|^2$ , and of the form  $\left(\frac{n-1}{n}\right)^2 e_\ell(T)$  for  $\|\mathbf{x}_n^{(t+T)}\|^2$ . Denote by  $D(T)$  the cumulative exponent for all  $(1, 1, n - 2)$  rows at layer  $t$ . Furthermore, denote by  $A(T)$  and  $B(T)$  the cumulative exponent for two-cluster rows with composition  $(1, n - 1)$  and  $(n - 1, 1)$  respectively, whose analysis was carried out in the proof of the two-cluster case in the main section. Following the discussion above, we get the following asymptotic formulas for large  $T$ ,

$$\|\mathbf{x}_1^{(t+T)}\|^2 \simeq \left(\frac{n-1}{n}\right)^2 A(T) + \frac{1}{n^2} B(T) + \left(\frac{n-1}{n}\right)^2 C(T) + \frac{1}{n^2} D(T) \quad (74)$$

$$\|\mathbf{x}_2^{(t+T)}\|^2 \simeq \frac{1}{n^2} A(T) + \frac{1}{n^2} B(T) + \frac{1}{n^2} C(T) + \frac{1}{n^2} D(T) \quad (75)$$

$$\|\mathbf{x}_n^{(t+T)}\|^2 \simeq \frac{1}{n^2} A(T) + \left(\frac{n-1}{n}\right)^2 B(T) + \frac{1}{n^2} C(T) + \left(\frac{n-1}{n}\right)^2 D(T) \quad (76)$$

from which it follows that, for large  $T$ ,

$$\frac{\|\mathbf{x}_2^{(t+T)}\|^2}{\|\mathbf{x}_1^{(t+T)}\|^2} \simeq \frac{1 + \frac{B(T)+D(T)}{A(T)+C(T)}}{(n-1)^2 + \frac{B(T)+D(T)}{A(T)+C(T)}} \quad (77)$$

$$\frac{\|\mathbf{x}_2^{(t+T)}\|^2}{\|\mathbf{x}_n^{(t+T)}\|^2} \simeq \frac{1 + \frac{A(T)+C(T)}{B(T)+D(T)}}{(n-1)^2 + \frac{A(T)+C(T)}{B(T)+D(T)}}. \quad (78)$$

As before, if  $\lim_{T \rightarrow \infty} \frac{A(T)+C(T)}{B(T)+D(T)} \geq 1$ , then

$$\lim_{t \rightarrow \infty} \frac{\|\mathbf{x}_2^{(t)}\|^2}{\|\mathbf{x}_1^{(t)}\|^2} \leq \frac{2}{(n-1)^2}, \quad (79)$$

otherwise,

$$\lim_{t \rightarrow \infty} \frac{\|\mathbf{x}_2^{(t)}\|^2}{\|\mathbf{x}_n^{(t)}\|^2} \leq \frac{2}{(n-1)^2}. \quad (80)$$

The proof for the fourth part follows similarly. Using the same notation, one has, for  $i \in \{3, n - 2\}$ ,

$$\langle \mathbf{x}_i^{(t+T)}, \mathbf{x}_1^{(t+T)} \rangle \simeq \frac{1}{n^2} B(T) + \frac{4}{n^2} D(T) \quad (81)$$

and

$$\langle \mathbf{x}_i^{(t+T)}, \mathbf{x}_n^{(t+T)} \rangle \simeq \frac{1}{n^2} A(T) + \frac{4}{n^2} C(T) \quad (82)$$

from which it follows that

$$\frac{\langle \mathbf{x}_i^{(t+T)}, \mathbf{x}_1^{(t+T)} \rangle}{\|\mathbf{x}_i^{(t+T)}\| \|\mathbf{x}_1^{(t+T)}\|} = \quad (83)$$

$$\simeq \frac{B(T) + 4D(T)}{\sqrt{A(T) + B(T) + 4C(T) + 4D(T)} \sqrt{(n-1)^2 A(T) + B(T) + (n-2)^2 C(T) + 4D(T)}} \quad (84)$$

$$\leq \frac{4}{\sqrt{\frac{A(T)+C(T)}{B(T)+D(T)} + 1} \sqrt{(n-2)^2 \frac{A(T)+C(T)}{B(T)+D(T)} + 1}} \quad (85)$$

and

$$\frac{\langle \mathbf{x}_i^{(t+T)}, \mathbf{x}_n^{(t+T)} \rangle}{\|\mathbf{x}_i^{(t+T)}\| \|\mathbf{x}_n^{(t+T)}\|} \lesssim \frac{4}{\sqrt{\frac{B(T)+D(T)}{A(T)+C(T)} + 1} \sqrt{(n-2)^2 \frac{B(T)+D(T)}{A(T)+C(T)} + 1}} \quad (86)$$

As before, for every  $T$  larger than a certain value, either  $\frac{A(T)+C(T)}{B(T)+D(T)} \leq 1$  or  $\frac{B(T)+D(T)}{A(T)+C(T)} \leq 1$ , from which we can conclude that either

$$\angle(\mathbf{x}_i^{(t)}, \mathbf{x}_1^{(t)}) \gtrsim \frac{\pi}{2} - \frac{\sqrt{2}\pi}{n-2} \quad (87)$$

or

$$\angle(\mathbf{x}_i^{(t)}, \mathbf{x}_n^{(t)}) \gtrsim \frac{\pi}{2} - \frac{\sqrt{2}\pi}{n-2}. \quad (88)$$

For the case  $i = 2$  (the case  $i = n - 1$  follows again by symmetry), let again  $A(T)$ ,  $B(T)$ ,  $C(T)$  and  $D(T)$  be the cumulative exponents for clusters with composition  $(1, n - 1)$ ,  $(n - 1, 1)$ ,  $(1, 1, n - 2)$ ,  $(n - 2, 1, 1)$  respectively. Notice that clusters with composition  $(1, 1, n - 2)$  asymptotically contribute only to  $\langle X_i^{(t+T)}, X_n^{(t+T)} \rangle$ , since point 1 and 2 get paired only when clusters of composition  $(2, n - 2)$  are formed in the process from layer  $t$  to  $t + T$ , which are asymptotically negligible per equation (62). The opposite is true for clusters of composition  $(n - 2, 1, 1)$ . Hence, asymptotically for large  $T$ , we have the formulae

$$\langle \mathbf{x}_2^{(t+T)}, \mathbf{x}_1^{(t+T)} \rangle \simeq \frac{1}{n^2} B(T) + \frac{1}{n^2} D(T) \quad (89)$$

$$\langle \mathbf{x}_2^{(t+T)}, \mathbf{x}_n^{(t+T)} \rangle \simeq \frac{1}{n^2} A(T) + \frac{1}{n^2} C(T) \quad (90)$$

from which it follows that

$$\frac{\langle \mathbf{x}_2^{(t+T)}, \mathbf{x}_1^{(t+T)} \rangle}{\|\mathbf{x}_2^{(t+T)}\| \|\mathbf{x}_1^{(t+T)}\|} \simeq \frac{1}{\sqrt{1 + (n-1)^2 \frac{A(T)+C(T)}{B(T)+D(T)}} \sqrt{1 + \frac{A(T)+C(T)}{B(T)+D(T)}}} \quad (91)$$

$$\frac{\langle \mathbf{x}_2^{(t+T)}, \mathbf{x}_n^{(t+T)} \rangle}{\|\mathbf{x}_2^{(t+T)}\| \|\mathbf{x}_1^{(t+T)}\|} \simeq \frac{1}{\sqrt{1 + (n-1)^2 \frac{B(T)+D(T)}{A(T)+C(T)}} \sqrt{1 + \frac{B(T)+D(T)}{A(T)+C(T)}}}. \quad (92)$$

Once again, if  $\lim_{T \rightarrow \infty} \frac{A(T)+C(T)}{B(T)+D(T)} \geq 1$ , then

$$\lim_{t \rightarrow \infty} \frac{\langle \mathbf{x}_2^{(t)}, \mathbf{x}_1^{(t)} \rangle}{\|\mathbf{x}_2^{(t)}\| \|\mathbf{x}_1^{(t)}\|} \leq \frac{1}{\sqrt{2}(n-1)}. \quad (93)$$

Otherwise,

$$\lim_{t \rightarrow \infty} \frac{\langle \mathbf{x}_2^{(t)}, \mathbf{x}_n^{(t)} \rangle}{\|\mathbf{x}_2^{(t)}\| \|\mathbf{x}_n^{(t)}\|} \leq \frac{1}{\sqrt{2}(n-1)}. \quad (94)$$

This concludes the proof of the theorem for the general case.

## Appendix F. Proof of Theorem 13 and Theorem 14

For both theorems, it is sufficient to calculate the expectation for a single row  $\mathbf{w}$  of  $W$ . This holds since the quantities of interest may be separated as a sum, where each summand corresponds to a unique row, and since all the rows are i.i.d each row has an equal contribution. For example, let us start by showing that norms of vectors may be scaled uniformly to our desire, in expectation, when choosing a suitable  $\sigma$ .

$$\mathbb{E} \|\text{ReLU}(W\mathbf{x})\|^2 = \mathbb{E} \text{ReLU}(W\mathbf{x}) \cdot \text{ReLU}(W\mathbf{x}) \quad (95)$$

$$= \mathbb{E} \sum_{i=1}^d \text{ReLU}(\mathbf{w}_i \mathbf{x}) \text{ReLU}(\mathbf{w}_i \mathbf{x}) \quad (96)$$

$$= \sum_{i=1}^d \mathbb{E} \text{ReLU}(\mathbf{w}_i \mathbf{x}) \text{ReLU}(\mathbf{w}_i \mathbf{x}) \quad (97)$$

$$= \frac{d\sigma^2}{2} \|\mathbf{x}\|^2 \quad (98)$$

The second equality follows from the definition of the scalar product, and the third equality is by the linearity of expectation. The fourth equality is less trivial and follows by noticing that  $N := \mathbf{w}_i \mathbf{x} \sim \mathcal{N}(0, \sigma^2 \|\mathbf{x}\|^2)$ . Since  $\text{ReLU}(x) = 0$  for negative  $x$ , we get that  $\mathbb{E} \text{ReLU}(N)^2 = \frac{1}{2} \mathbb{E} N^2 = \frac{\sigma^2 \|\mathbf{x}\|^2}{2}$ . The computation above was independent of  $\mathbf{x}$ . So,  $\sigma$  allows us to change the scale of all vector norms simultaneously.

We now prove Theorem 13 by proving each item of Definition 12 for  $\mathbb{E} X^{(t+1)}$ . Denote  $\tilde{\mathbf{x}}_i = \mathbf{x}_i - \frac{1}{n} \sum_{j=1}^n \mathbf{x}_j$  for  $1 \leq i \leq n$  and  $\tilde{\mathbf{x}}_{n+1} = \boldsymbol{\nu}_c - \frac{1}{n} \sum_{j=1}^n \mathbf{x}_j$ . We now examine the geometry of  $\{\tilde{\mathbf{x}}_i\}_{i=1}^n$ . To that end, we choose a coordinate system where  $\mathbf{x}_1 = (1, 0, \dots, 0)$  and  $\boldsymbol{\nu}_c = (0, \frac{1}{n-1}, 0, \dots, 0)$ . We may choose any coordinate system because we calculate the expectation over a Gaussian distribution which is spherically symmetric, and the choice we made is allowed since  $\mathbf{x}_1$  and  $\boldsymbol{\nu}_c$  are orthogonal.

Then,

$$\tilde{\mathbf{x}}_1 = \mathbf{x}_1 - \frac{1}{n} \sum_{i=1}^n \mathbf{x}_i \quad (99)$$

$$= \mathbf{x}_1 - \frac{1}{n} \mathbf{x}_1 - \frac{n-1}{n} \boldsymbol{\nu}_c \quad (100)$$

$$= \left( \frac{n-1}{n}, -\frac{1}{n}, 0, \dots, 0 \right) \quad (101)$$

and similarly,

$$\tilde{\mathbf{x}}_{n+1} = \boldsymbol{\nu}_c - \frac{1}{n} \sum_{i=1}^n \mathbf{x}_i \quad (102)$$

$$= \boldsymbol{\nu}_c - \frac{1}{n} \mathbf{x}_1 - \frac{n-1}{n} \boldsymbol{\nu}_c \quad (103)$$

$$= \left( -\frac{1}{n}, \frac{1}{n(n-1)}, 0, \dots, 0 \right). \quad (104)$$

Hence,

$$\|\tilde{\mathbf{x}}_1\|^2 = \frac{n^2 - 2n + 2}{n^2} \quad \text{and} \quad \|\tilde{\mathbf{x}}_{n+1}\|^2 = \frac{n^2 - 2n + 2}{n^2 (n-1)^2}$$

This shows that if we pick  $\sigma^2 = \frac{2\alpha}{d}$ , we have proved item 1 since

$$\mathbb{E} \left\| \mathbf{x}_1^{(t+1)} \right\|^2 = \mathbb{E} \operatorname{ReLU} \left( W \mathbf{x}_1 - \boldsymbol{\mu}^{(t)} \right) \cdot \operatorname{ReLU} \left( W \mathbf{x}_1 - \boldsymbol{\mu}^{(t)} \right) \quad (105)$$

$$= \mathbb{E} \operatorname{ReLU} \left( W \tilde{\mathbf{x}}_1 \right) \cdot \operatorname{ReLU} \left( W \tilde{\mathbf{x}}_1 \right) \quad (106)$$

$$= \frac{d\sigma^2}{2} \|\tilde{\mathbf{x}}_1\|^2 = 1, \quad (107)$$

and similarly, item 2 since

$$\mathbb{E} \|\hat{\boldsymbol{\nu}}_c\|^2 = \mathbb{E} \operatorname{ReLU} \left( W \boldsymbol{\nu}_c - \boldsymbol{\mu}^{(t)} \right) \cdot \operatorname{ReLU} \left( W \boldsymbol{\nu}_c - \boldsymbol{\mu}^{(t)} \right) \quad (108)$$

$$= \mathbb{E} \operatorname{ReLU} \left( W \tilde{\mathbf{x}}_{n+1} \right) \cdot \operatorname{ReLU} \left( W \tilde{\mathbf{x}}_{n+1} \right) \quad (109)$$

$$= \frac{d\sigma^2}{2} \|\tilde{\mathbf{x}}_{n+1}\|^2 = \frac{1}{(n-1)^2}. \quad (110)$$

Item 3 follows from two simple observations:

- $\angle(\tilde{\mathbf{x}}_1, \tilde{\mathbf{x}}_{n+1}) = \pi$
- If  $\mathbf{u}, \mathbf{v}$  are vectors such that  $\mathbf{u} = -a\mathbf{v}$  for  $a > 0$ , then  $\operatorname{ReLU}(\mathbf{u}) \cdot \operatorname{ReLU}(\mathbf{v}) = 0$ .



So, by the first observation we have  $\tilde{\mathbf{x}}_1 = -a\tilde{\mathbf{x}}_{n+1}$  for some  $a > 0$ . So,  $W\tilde{\mathbf{x}}_1 = -aW\tilde{\mathbf{x}}_{n+1}$  holds for any  $W$ . The second observation then implies

$$\mathbf{x}_1^{(t+1)} \cdot \hat{\nu}_c = \text{ReLU}(W\tilde{\mathbf{x}}_1) \cdot \text{ReLU}(W\tilde{\mathbf{x}}_{n+1}) = 0,$$

which concludes the proof of item 3.

Finally, item 4 is trivial since  $\mathbf{x}_i = \nu_c$  for all  $2 \leq i \leq n$  and  $f(\mathbf{x}) = \mathbb{E} \text{ReLU}(W\mathbf{x} - \boldsymbol{\mu}^{(t)})$  is a function of  $\mathbf{x}$ .

The proof of items 1, 2, and 3 of Theorem 14 follows the same lines of the proof for Theorem 13, this time with  $\alpha = \frac{n^2}{(n-1)^2 R^2}$ .

For item 4, we require a more intricate expectation calculation than in equation 95. We need the expected inner product between  $\text{ReLU}(W\mathbf{x})$  and  $\text{ReLU}(W\mathbf{y})$ . By equation 6 in Cho and Saul (2009) we have:

$$\mathbb{E} \text{ReLU}(W\mathbf{x}) \cdot \text{ReLU}(W\mathbf{y}) = \frac{d\sigma^2 \|\mathbf{x}\| \|\mathbf{y}\| \sqrt{1 - \rho^2} + (\pi - \cos^{-1}(\rho)) \rho}{2\pi} := K(\mathbf{x}, \mathbf{y}) \quad (111)$$

where  $\rho := \frac{\mathbf{x} \cdot \mathbf{y}}{\|\mathbf{x}\| \|\mathbf{y}\|}$  is the similarity between vectors  $\mathbf{x}$  and  $\mathbf{y}$ .

The function appearing in equation 111 has an important property:

$$K(\mathbf{x}, \mathbf{y}) > \mathbf{x} \cdot \mathbf{y}$$

for  $\sigma^2 = \frac{2}{d}$  and  $\mathbf{x} \neq \mathbf{y}$ .

For  $\mathbf{x}_i \neq \mathbf{x}_j$ , this property implies that for  $\sigma^2 = \frac{2}{d}$  we have:

$$\|\mathbf{x}_i - \mathbf{x}_j\|^2 = \|\tilde{\mathbf{x}}_i - \tilde{\mathbf{x}}_j\|^2 \quad (112)$$

$$= \|\tilde{\mathbf{x}}_i\|^2 + \|\tilde{\mathbf{x}}_j\|^2 - 2\tilde{\mathbf{x}}_i \cdot \tilde{\mathbf{x}}_j \quad (113)$$

$$= \mathbb{E} \left\| \text{ReLU}(W\mathbf{x}_i - \boldsymbol{\mu}^{(t)}) \right\|^2 + \left\| \text{ReLU}(W\mathbf{x}_j - \boldsymbol{\mu}^{(t)}) \right\|^2 - 2\tilde{\mathbf{x}}_i \cdot \tilde{\mathbf{x}}_j \quad (114)$$

$$> \mathbb{E} \left\| \text{ReLU}(W\mathbf{x}_i - \boldsymbol{\mu}^{(t)}) \right\|^2 + \left\| \text{ReLU}(W\mathbf{x}_j - \boldsymbol{\mu}^{(t)}) \right\|^2 - 2K(\tilde{\mathbf{x}}_i, \tilde{\mathbf{x}}_j) \quad (115)$$

$$= \mathbb{E} \left\| \text{ReLU}(W\mathbf{x}_i - \boldsymbol{\mu}^{(t)}) - \text{ReLU}(W\mathbf{x}_j - \boldsymbol{\mu}^{(t)}) \right\|^2 \quad (116)$$

$$= \mathbb{E} \left\| \mathbf{x}_i^{(t+1)} - \mathbf{x}_j^{(t+1)} \right\|^2 \quad (117)$$

The result also holds if we take  $\sigma^2 = \frac{2\alpha}{d}$  with  $\alpha = \frac{n^2}{(n-1)^2 R^2}$ . This is because ReLU is homogeneous  $\text{ReLU}(\alpha x) = \alpha \text{ReLU}(x)$  for  $\alpha > 0$ , so that we have

$$\mathbb{E} \left\| \mathbf{x}_i^{(t+1)} - \mathbf{x}_j^{(t+1)} \right\|^2 < \alpha \|\mathbf{x}_i - \mathbf{x}_j\|^2 < \|\mathbf{x}_i - \mathbf{x}_j\|^2$$

since  $\alpha < 1$ . This concludes the proof of item 4.